Title: Guidelines on experimental methods to assess mitochondrial dysfunction in cellular models of neurodegenerative diseases

Running title: Methods to assess neuronal mitochondrial dysfunction

Niamh M. C. Connolly[1], Pierre Theurey[2], Vera Adam-Vizi[17], Nicolas G. Bazan[Error! Reference source not found.], Paolo Bernardi[2,34], Juan P. Bolaños[15], Carsten Culmsee[Error! Reference source not found.], Valina L. Dawson[7,32], Mohanish Deshmukh[27], Michael R. Duchen[8], Heiko Düssmann[1], Gary M. Fiskum[18,29], Maria F. Galindo[33], Giles E. Hardingham[16], J. Marie Hardwick[Error! Reference source not found.], Mika B. Jekabsons[11], Elizabeth A. Jonas[Error! Reference source not found.], Joaquin Jordán[Error! Reference source not found.], Stuart A. Lipton[13], Giovanni Manfredi[28], Mark P. Mattson[6], BethAnn McLaughlin[26], Axel Methner[14], Anne N. Murphy[35], Michael P. Murphy[12], David G. Nicholls[Error! Reference source not found.], Brian M. Polster[18], Tullio Pozzan[2,34], Rosario Rizzuto[2], Ruth S. Slack[4], Jorgina Satrústegui[Error! Reference source not found.], Raymond A. Swanson[10], Russell Swerdlow[19], Yvonne Will[Error! Reference source not found.], Zheng Ying[30], Alvin Joselin[4], Anna Gioran[5], Catarina Moreira Pinho[3], Orla Watters[1], Manuela Salvucci[1], Irene Llorente-Folch[1], David S. Park[4], Daniele Bano[5], Maria Ankarcrona[3], Paola Pizzo[2,34], Jochen H. M. Prehn[1*]

[1] Dept. of Physiology & Medical Physics, Royal College of Surgeons in Ireland, Dublin, Ireland.

[2] Dept. of Biomedical Sciences, University of Padova, Padova, Italy.

[3] Center for Alzheimer Research, Division of Neurogeriatrics, Department of Neurobiology, Care Sciences and Society, Karolinska Institutet, Stockholm, Sweden.

[4] Brain & Mind Research Institute, University of Ottawa, Ontario K1H 8M5, Canada.

[5] German Center for Neurodegenerative Diseases (DZNE), Bonn, Germany.

[6] National Institute on Aging Intramural Research Program, Baltimore, MD, USA.

[7] Neuroregeneration and Stem Cell Programs, Institute for Cell Engineering; Dept. of Physiology; Dept. of Neurology; Solomon H. Snyder Dept. of Neuroscience, Johns Hopkins University School of Medicine, Baltimore, MD 21205, USA.

[8] Dept. of Cell and Developmental Biology and Consortium for Mitochondrial Research, University College London, London WC1E 6BT, UK.

[9] Buck Institute for Research on Aging, Novato, CA 94945, USA.

[10] Dept. of Neurology, University of California San Francisco and San Francisco Veterans Affairs Medical Center, San Francisco, CA94121, USA.

[11] Dept. of Biology, University of Mississippi, University, MS 38677, USA.

[12] MRC Mitochondrial Biology Unit, University of Cambridge, Cambridge Biomedical Campus, CB2 0XY, UK.

[13] Neuroscience Translational Center and Dept. of Molecular Medicine, The Scripps Research Institute, La Jolla, CA 92037, USA; Neurodegenerative Disease Center, Scintillon Institute, San Diego, CA 92121, USA; Department of Neurosciences, University of California San Diego, School of Medicine, La Jolla, CA 92093, USA.

[14] University Medical Center Mainz, Dept. of Neurology, Mainz, Germany.

[15] University of Salamanca, CIBERFES, Institute of Functional Biology and Genomics (IBFG), CSIC, 37007 Salamanca, Spain.

[16] UK Dementia Research Institute at the University of Edinburgh, Edinburgh Medical School, Edinburgh EH8 9XD, UK.

[17] Dept. of Medical Biochemistry, Semmelweis University, Budapest, Hungary.

[18] Dept. of Anesthesiology and Center for Shock, Trauma and Anesthesiology Research (STAR), University of Maryland School of Medicine, Baltimore, MD 21201, USA.

[19] The University of Kansas Alzheimer's Disease Center and Depts. of Neurology, Molecular and Integrative Physiology, and Biochemistry and Molecular Biology, University of Kansas Medical Center, Kansas City, Kansas 66160, USA.

[20] Pfizer, Groton, CT 06340, USA.

[21] Neuroscience Center of Excellence, School of Medicine, Louisiana State University Health Sciences Center, New Orleans, LA, USA.

[22] Dept. Of Medical Science-Pharmacology, University of Castilla-La Mancha, Albacete, Spain.

[23] Dept. of Molecular Microbiology and Immunology, Johns Hopkins University, Bloomberg School of Public Health, Baltimore, MD 21205, USA.

[24] Dept. of Internal Medicine, Section of Endocrinology, Yale University, New Haven, CT, USA.

[25] Institute of Pharmacology and Clinical Pharmacy, University of Marburg, 35043 Marburg, Germany.

[26] Dept. of Neurology, Vanderbilt University School of Medicine, Nashville, TN, USA.

[27] Neuroscience Center, University of North Carolina, Chapel Hill, USA.

[28] Brain and Mind Research Institute, Weill Cornell Medicine, NY 10065, USA.

[29] Program in Neuroscience, University of Maryland School of Medicine, Baltimore, USA.

[30] Laboratory of Cellular and Molecular Neuropharmacology, Jiangsu Key Laboratory of Translational Research and Therapy for Neuro-Psycho-Diseases and College of Pharmaceutical Sciences, Soochow University, Suzhou, Jiangsu 215021, China.

[31] Dpto. de Biología Molecular, Centro de Biología Molecular Severo Ochoa, Consejo Superior de Investigaciones Científicas-Universidad Autónoma de Madrid, 28049 Madrid, Spain.

[32] Adrienne Helis Malvin Medical Research Foundation; Diana Helis Henry Medical Research Foundation, New Orleans, LA 70130, USA.

[33] Unidad de Neuropsicofarmacología Translacional, Complejo Hospitalario Universitario de Albacete, Albacete, Spain.

[34] Neuroscience Institute, National Research Council (CNR), Padova, Italy.

[35] Dept. of Pharmacology, University of California, San Diego, CA 92093, USA.

*** Corresponding author**: Prof. Jochen Prehn, Professor of Physiology, Dept. of Physiology & Medical Physics, Royal College of Surgeons in Ireland, 123 St. Stephen's Green, Dublin 2, Ireland. Tel.: +353-1-402-2255. Email: prehn@rcsi.ie

1. Abstract

Neurodegenerative diseases are a spectrum of chronic, debilitating disorders characterised by the progressive degeneration and death of neurons. Mitochondrial dysfunction has been implicated in most neurodegenerative diseases, but in many instances it is unclear whether such dysfunction is a cause or an effect of the underlying pathology, and whether it represents a viable therapeutic target. It is therefore imperative to utilise and optimise cellular models and experimental techniques appropriate to determine the contribution of mitochondrial dysfunction to neurodegenerative disease phenotypes. In this consensus article, we collate details on and discuss pitfalls of existing experimental approaches to assess mitochondrial function in *in vitro* cellular models of neurodegenerative diseases, including specific protocols for the measurement of oxygen consumption rate in primary neuron cultures, and single-neuron, time-lapse fluorescence imaging of the mitochondrial membrane potential and mitochondrial NAD(P)H. As part of the Cellular Bioenergetics of Neurodegenerative Diseases (CeBioND) consortium (www.cebiond.org), we are performing cross-disease analyses to identify common and distinct molecular mechanisms involved in mitochondrial bioenergetic dysfunction in cellular models of Alzheimer's, Parkinson's and Huntington's diseases. Here we provide detailed guidelines and protocols as standardised across the five collaborating laboratories of the CeBioND consortium, with additional contributions from other experts in the field.

2. Bullet Points

- It is important to utilise and optimise appropriate cellular models and experimental techniques to determine the contribution of mitochondrial dysfunction to neurodegenerative disease.
- Here, we provide guidelines on techniques to investigate mitochondrial function in cellular models of neurodegenerative diseases, including detailed protocols for the measurement of oxygen consumption rate in primary neuron cultures, and single-neuron, time-lapse fluorescence imaging of the mitochondrial membrane potential and mitochondrial NAD(P)H.
- The protocols and guidelines provided here will enable analysis of primary and secondary mitochondrial dysfunction in neurodegenerative diseases, allowing experimental comparison between laboratories and optimising translation of *in vitro* findings to *in vivo* studies.

3. Introduction

Neurodegenerative diseases (NDs) comprise a spectrum of heterogeneous pathologies involving the progressive dysfunction, degeneration, and death of neurons, leading to incurable and debilitating conditions. Although some genetic factors have been identified, the underlying pathophysiology behind familial and sporadic NDs remains poorly understood. Of note, nearly all NDs exhibit impaired mitochondrial energy metabolism (Johri and Beal, 2012, Pathak et al., 2013, Lin and Beal, 2006). For example, studies have repeatedly demonstrated reduced expression and impaired activity of respiratory chain Complex I in Parkinson's disease (PD), Complex IV in Alzheimer's disease (AD), and Complexes II and III in Huntington's disease (HD), and reduced activity of α-ketoglutarate dehydrogenase in both AD and PD (Yin et al., 2014). Drug-induced models of NDs further link respiratory complex deficiency with disease – rotenone and MPTP (1-methyl-4-phenyl-1,2,3,6-tetrahydropyridine), both inhibitors of Complex I, cause Parkinson-related pathology in animal models (Martinez and Greenamyre, 2012), and 3-nitropropionic acid (3-NP), a Complex II inhibitor, produces a HD phenotype in mice (Brouillet et al., 1999). Several gene mutations associated with NDs affect proteins that contribute to mitochondrial homeostatic regulation and function (**Error! Reference source not found.**). Whether these mitochondria-associated dysfunctions are sufficient to cause neurodegenerative pathogenesis, however, remains uncertain, as they may also evolve secondary to a different underlying pathology (Polyzos and McMurray, 2017). Indeed, a decline in mitochondrial function may be a natural process of ageing, but may usually be compensated for by adaptive changes (Yin et al., 2014, Swerdlow et al., 2014, Raefsky and Mattson, 2017). A loss of these compensatory mechanisms, or a 'second trigger' (such as genetic predisposition, endogenous/exogenous toxins or chronic excitotoxicity), may convert any natural subclinical decline into a clinically relevant neurodegenerative phenotype ('dual/two/double-hit' hypotheses (Sulzer, 2007, Zhu et al., 2007)). Clearly, extensive work is still required to thoroughly investigate the cause and impact of mitochondrial dysfunction in NDs.

It is currently difficult to compare and contrast the vast volumes of experimental research in cellular models of NDs due to methodological differences – cell and neuron type, age, method of preparation and culture, equipment/assays, experimental set-up, outputs measured – as well as due to limited detail in method reporting. These discrepancies may compound the difficulties in translating experimental findings from *in vitro* cellular models to *in vivo* or human studies. Here, we provide guidelines on several experimental methods to assess mitochondrial dysfunction in *in vitro* cellular models of NDs, with the goal of reducing methodological differences between research laboratories. The CeBioND consortium (www.cebiond.org) is performing cross-disease analyses to investigate mitochondrial bioenergetic dysfunction in cellular models of AD, PD and HD. Within this consortium, we standardised single-cell fluorescence protocols (TMRM, NAD(P)H autofluorescence)

and oxygen consumption rate measurements across five collaborating laboratories. These protocols are detailed here. For this consensus review, we recruited several experts from the field of mitochondrial research to contribute details on additional techniques for a thorough evaluation of mitochondrial function and dysfunction. Collectively, we have developed guidelines that suit most biological laboratories and that provide for a standardised, holistic assessment of mitochondrial function in cellular models of a variety of NDs.

*Table 1: Proteins/genes known to be mutated in Alzheimer's disease (AD), Parkinson's disease (PD), Frontotemporal dementia (FTD), Huntington's disease (HD) and Amyotrophic Lateral Sclerosis (ALS). Several of these genes (*PSEN1/2*;* SNCA, DJ-1, LRRK2, Parkin, PINK-1; MAPT*;* Htt*;* SOD1, FUS, TARDP, and CHCHD10*) encode proteins that regulate mitochondrial homeostasis and function to varying degrees (Martinez and Greenamyre, 2012, Gao et al., 2017, Schon and Przedborski, 2011, Lin and Beal, 2006). Listed genes are commonly targeted in transgenic animal models - see http://www.neurodegenerationresearch.eu/initiatives/jpnd-alignment-actions/animal-and-cell-models/, http://www.alzforum.org/research-models, (Gotz and Ittner, 2008, Harvey et al., 2011), and references therein for further details. The ALS-associated genes* FUS, TARDBP, C9orf72 *and* CHCHD10 *are also associated with FTD.*

Disease	**Protein (*Gene*)**
AD	Amyloid precursor protein (*APP*)
	Apolipoprotein E *(APOE*)
	Microtubule associated protein tau (*MAPT*)
	Presenilin (*PSEN1/2*)
PD	α-synuclein (*SNCA*)
	DJ-1 (*DJ-1/PARK7*)
	Leucine-rich repeat kinase 2 (*LRRK2*)
	Parkin (*Parkin)*
	PTEN-induced kinase 1 (*PINK-1)*
FTD	Microtubule associated protein tau (*MAPT*)
HD	Huntingtin (*Htt/IT15*)
ALS	Superoxide Dismutase (*SOD-1*)
	DNA/RNA binding protein Fused in Sarcoma (*FUS*)
	(TAR)-DNA-binding protein 43 (*TARDBP*)
	C9orf72 (*C9orf72*)
	Coiled-coil-helix-coiled-coil-helix domain-containing protein 10 (*CHCHD10*)

4. Mitochondrial bioenergetic processes

The components of mitochondrial bioenergetics are described in most biochemistry textbooks, and we provide only a brief introduction here. Although mitochondria are crucially involved in apoptosis, calcium signalling, lipid biosynthesis, synthesis of haem and iron sulphur centres, carbohydrate and fatty acid metabolism, and redox homeostasis, the most celebrated function of mitochondria is oxidative phosphorylation (OxPhos), the oxygen-dependent production of ATP driven by an electrochemical gradient across the inner mitochondrial membrane. Neurons are heavily dependent on OxPhos, especially in times of increased energy demand (Connolly et al., 2014, Herrero-Mendez et al., 2009), and are therefore highly sensitive to loss of substrate or other impairments in the processes underlying OxPhos (Kann and Kovacs, 2007).

Mitochondrial ATP synthesis is driven by the maintenance of a proton circuit comprising the respiratory/electron transport chain, the F_1F_o ATP synthase, and proton leaks. The multi-subunit complexes of the respiratory chain (forming the respirasome) reside within the inner mitochondrial membrane and consist of Complex I (NADH:ubiquinone oxidoreductase/NADH dehydrogenase), Complex II (succinate-ubiquinone oxidoreductase/succinate dehydrogenase), Complex III (ubiquinol-cytochrome *c* oxidoreductase) and the O_2 consuming Complex IV (cytochrome *c* oxidase). Protons (H^+) pumped out of the mitochondrial matrix by these respiratory complexes, coupled with electron transport through the complexes, maintain the electrochemical proton-motive force (Δp) which comprises a H^+ concentration gradient (ΔpH_m) and an electrical gradient (the mitochondrial membrane potential, $\Delta\psi_m$) across the inner membrane (Mitchell and Moyle, 1969, Nicholls and Ferguson, 2013). These gradients allow H^+ to flow back into the matrix through the F_1F_o ATP synthase, with the resultant synthesis of ATP from ADP and phosphate. The H^+ circuit can also be completed by inducible or non-inducible H^+ leaks across the inner membrane, bypassing the F_1F_o ATP synthase (Jastroch et al., 2010). Mitochondrial NADH, generated by the tricarboxylic acid (TCA) cycle within the mitochondrial matrix or via the import of NADH-derived reducing equivalents driven by the malate-aspartate shuttle, serves as an electron donor for the respiratory chain. The activity of Complex II, which, through the oxidation of succinate to fumarate reduces ubiquinone to ubiquinol, also enables electron transfer to Complex III. Reactive oxygen species (ROS), produced in mitochondria by the TCA cycle and respiratory chain, are vital second messengers, but their overproduction can lead to oxidative stress.

5. Methods to assess mitochondrial dysfunction in cellular models of neurodegenerative diseases

Here we provide detailed guidelines on experimental techniques to investigate mitochondrial bioenergetics in *in vitro* cellular models, including specific protocols to measure the oxygen consumption rate, the mitochondrial membrane potential and mitochondrial NAD(P)H. Analysis of mitochondrial transport, network morphology, fusion/fission, mitophagy and biogenesis, factors that are also altered in NDs (Johri and Beal, 2012, Gao et al., 2017, Schon and Przedborski, 2011, Aouacheria et al., 2017), are beyond the scope of the present work. While cellular models are not optimal experimental systems, as they often lack the multi-cellular environment of intact *in vivo* models, they provide a relatively simple environment within which complex molecular interactions can be thoroughly studied at a population and single-cell level.

5.1. Cellular models (experimental systems) of neurodegenerative diseases

The anatomical, neurochemical and metabolic uniqueness of primary neuron cultures derived from rodents (mice and rats) offer a currently unparalleled platform for the study of the molecular mechanisms of neurodegeneration. Primary neurons can be cultured from wild-type or transgenic animals to generate relatively homogenous neuronal populations for study *in vitro* (***Error! Reference source not found.***). Protocols for the preparation and culture of various neuronal populations are available (Hilgenberg and Smith, 2007, Sciarretta and Minichiello, 2010, Fairbanks et al., 2013). Primary neurons from specific brain regions may be the ideal cellular model (e.g. dopaminergic neurons for PD, hippocampal neurons for AD, striatal neurons for HD, motor neurons for ALS), but are less abundant and not always easy to prepare nor culture. Variations in the preparation and culture of primary neuron cultures, such as the age and sex of the animals, seeding density, days *in vitro*, media/buffer composition and substrate availability, may alter neuronal physiology, mitochondrial function and viability, and contribute to heterogeneity in experimental results (Kleman et al., 2008, Zhu et al., 2012, Surin et al., 2012, Fairbanks et al., 2013, Biffi et al., 2013).

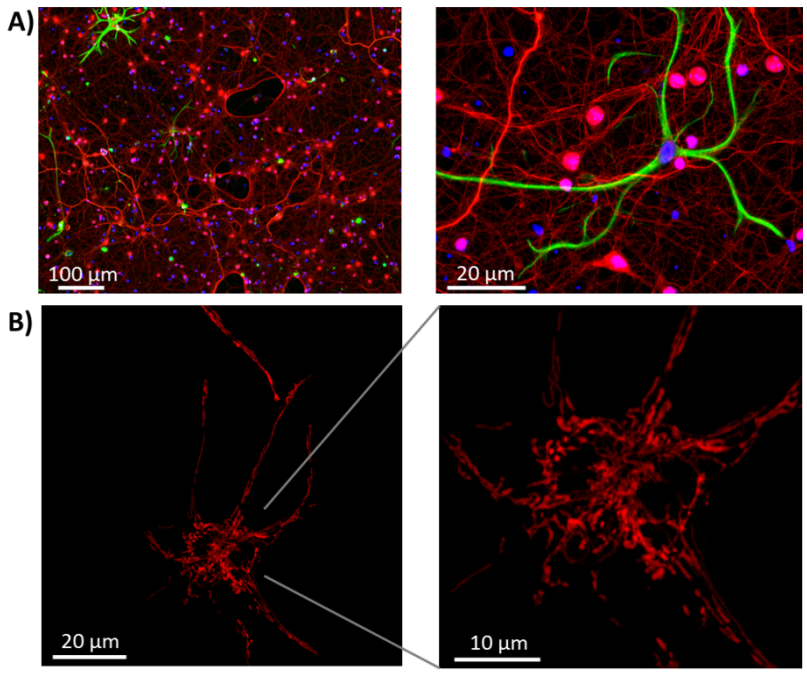

Figure 1: Immunofluorescent labelling and fluorescent images of cortical neurons prepared from post-natal wild-type mice. A) After 10 days in vitro *(DIV), cultures were stained with antibodies against the neuron-specific NF200 (red) and the astrocyte-specific GFAP (green), and with the DNA dye Hoechst (blue). Even when moved to a serum-free media quickly after dissociation, neuronal cultures contain a small proportion of astrocytes and other cell types (such as fibroblasts and endothelial cells). Neurons can be morphologically identified when performing single-cell experiments (Abramov et al., 2007), but regular and careful characterisation of cultures is important for cell population assays. B) Cortical neurons (after 6 DIV) transfected with a mitochondrial red fluorescent protein highlight the intricate mitochondrial network throughout the neuron.*

Brain-derived cell lines, such as the human SH-SY5Y or the rodent PC12, N2a and HT22, can be differentiated to a post-mitotic neuronal state (Constantinescu et al., 2007, Greene and Tischler, 1976, Tremblay et al., 2010), but they do not exhibit a true neuronal phenotype (e.g. they lack functional NMDA receptors even after differentiation), and their bioenergetics and neurotoxic properties differ from primary neurons (LePage et al., 2005). Although their ease of culturing and transfection make them a feasible compromise between convenience and scientific relevance, findings in these cellular models should be complemented with experiments in primary cultures or *in vivo* models. Neurons can also be differentiated from proliferative cell types, such as neural progenitor cells (NPCs) from the sub-ventricular zone of adult mice. More recently, cellular models of disease have been derived from patient cells. Dopaminergic, motor, striatal and forebrain neurons derived from induced pluripotent stem cells (iPSCs) reprogrammed from human fibroblasts have been used to investigate PD, ALS, HD

and AD, respectively (Hung et al., 2017), although iPSCs still require expensive and labour-intensive techniques. It is important to use isogenically-corrected iPSCs as a control when studying the effects of genetic mutations on mitochondrial properties; CRISPR/Cas9, TALEN or other techniques can be used to correct the mutation (Ryan et al., 2013). 3-D culture models developed using neural cells can recapitulate multiple aspects of ND pathologies (Choi et al., 2016). Primary astrocyte, microglia and associated cell cultures are also relevant cellular models, specifically to study non-cell autonomous and inflammatory processes, which may contribute significantly to the progression of NDs (Schlachetzki et al., 2013).

The experimental methods described herein focus on primary neuronal cultures, but can be performed in most cellular models. Decisions on specific cellular models and experimental design depend on the research question and on the available equipment, reagents, and expertise. Regardless, conditions should remain as similar as possible for all experiments within a study, and matched experiments (control and treated, or wild-type and transgenic littermates) should always be performed, ideally on the same day. Maintaining consistency both within a study and across platforms will facilitate inter-experiment comparison.

For live cell imaging, neurons should be equilibrated in 'experimental buffer' for at least 30 minutes - we find that (in mM) 120 NaCl, 3.5 KCl, 0.4 KH_2PO_4, 5 $NaHCO_3$, 20 HEPES, 1.2 Na_2SO_4, at pH 7.4 (slightly higher than normal brain extracellular pH of ~7.2-7.3) works well for experiments on primary cortical and other central neurons, supplemented with 1-2 mM $MgCl_2$ to reduce neuronal activity, 1.2 mM $CaCl_2$, and the desired energy substrate (e.g. glucose, pyruvate, lactate, glutamine). The type and concentration of energy substrate will critically determine metabolic behaviour, and similar measurements performed with different substrates are not directly comparable. Neurons should be equilibrated at 37 °C, in the dark if utilising fluorescent reporters, and with no CO_2 if the buffer contains HEPES or equivalent.

Table 2: Drugs targeting the mitochondrial bioenergetic machinery. Concentrations are guidelines only for primary neurons, and should be optimised for each cell type or experimental setting. Changes to the experimental buffer, such as the inclusion of bovine serum albumin, can alter some of the effective drug concentrations by more than 4-fold (Jekabsons and Nicholls, 2004, Clerc and Polster, 2012). High protonophore concentrations collapse the mitochondrial membrane potential (and may also depolarise the plasma membrane potential (Nicholls, 2006)), while low concentrations induce maximal respiration (this requires titration to determine the optimal concentration for each experimental set-up (Brand and Nicholls, 2011, Dranka et al., 2011)). References for concentrations were obtained from experiments in primary neurons: (Duan et al., 2000, Ward et al., 2000, Bizat et al., 2005, Abramov et al., 2007, Brennan et al., 2009, Chinopoulos et al., 2010, Llorente-Folch et al., 2013, Rueda et al., 2015). 3-NP – 3-Nitropropionic acid, FCCP – Carbonyl cyanide-4-(trifluoromethoxy)phenylhydrazone, CCCP – Carbonyl cyanide m-chlorophenylhydrazone, DNP – 2,4-dinitrophenol.

Target	**Drug**	**Concentrations (primary neurons)**	**Off-target effects**
Complex I inhibition	Rotenone	1-2 μM	Microtubules
Complex II inhibition	3-NP	0.1-1 mM	
Complex III inhibition	Antimycin A	1-3 μM	Aspecific permeabilisation of the inner mitochondrial membrane
	Stigmatellin	1-3 μM	Also inhibits Complex I at high concentrations
	Myxothiazol	1-5 μM	Also inhibits Complex I at high concentrations
Complex IV inhibition	Cyanide (NaCN, KCN)	1-5 mM	Haem-containing enzymes; formation of thiocyanate adducts
	Sodium Azide	1-5 mM	Interacts with active groups from catalase and nitrogen-based structures
F_1F_o ATP Synthase inhibition	Oligomycin	1-5 μg/ml (1-6 μM)*	
Protonophore (increases proton leak; uncouples mitochondria)	FCCP	High: 10 μM Low: 0.3-1 μM	
	CCCP	High: 10 μM Low: 0.3-1 μM	Inhibits lysosomes and autophagy

	DNP	Low: 0.1-0.5 mM

* Oligomycin concentrations are often listed as μg/ml, as commercial preparations are a mixture of compounds with different individual molecular weights.

5.2. Measurement of the oxygen consumption rate (OCR)

Oxygen consumption is an excellent read-out for mitochondrial respiratory activity. Measurement of the oxygen consumption rate (OCR) is the current experiment of choice to determine underlying mitochondrial dysfunction (Brand and Nicholls, 2011, Dranka et al., 2011). Although Complex IV is the only oxygen consumer within the proton circuit, appropriate pharmacological manipulation can isolate different respiratory states and facilitate modularised assessment of the complete circuit, including basal respiration, maximal respiration, proton leak and ATP turnover (

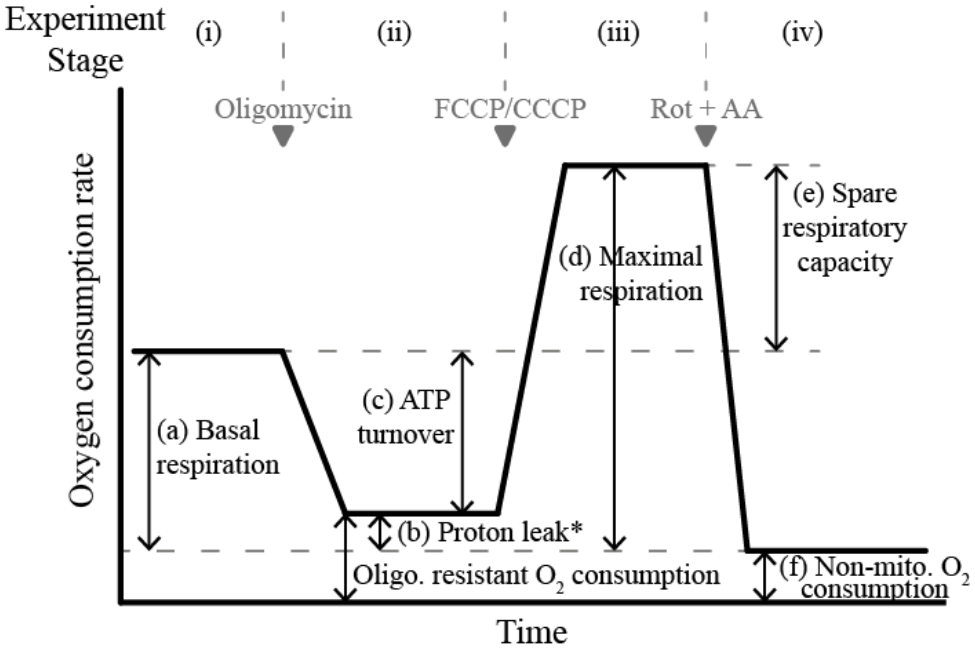

Figure 2).

The OCR has been extensively studied in various cellular models of NDs (Polyzos and McMurray, 2017, Rhein et al., 2009, Chakraborty et al., 2016). It can be measured in isolated mitochondria or permeabilised cells following a slightly altered protocol to the one described below (initial addition of ADP, phosphate and substrate to initiate pure 'State 3' respiration (Brand and Nicholls, 2011)), or in intact cells or brain slices. Mitochondria isolation is a delicate procedure that provides a precise and controllable model at the expense of physiological relevance, while brain slices, which maintain intact neuronal networks, constitute a more complete biological system. In whole cells, optimised permeabilisation of the plasma membrane allows controlled supply of substrate to mitochondria, providing a more controllable model without complete loss of the cytosolic milieu (Clerc and Polster, 2012, Salabei et al., 2014). The measurement of OCR in permeabilised cells or isolated mitochondria provided with different substrates (e.g. the provision of glutamate/malate to drive flux through Complex I, or succinate to drive flux through Complex II) can isolate specific complex activity and help to identify the molecular origin of a mitochondrial defect (Salabei et al., 2014).

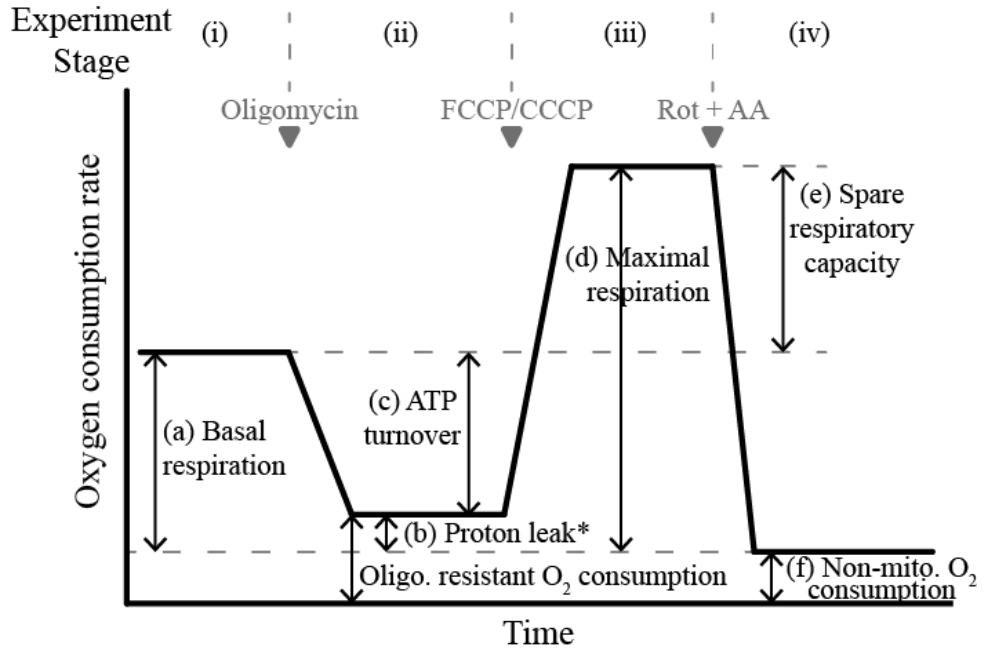

*Figure 2: Schematic of standard experimental protocol to investigate the contribution of components of the mitochondrial respiratory chain to the oxygen (O_2) consumption rate (OCR). Mitochondrial function can be thoroughly investigated in intact cells by measuring the OCR during sequential addition of mitochondrial respiratory inhibitors (marked with grey triangles). The different stages of the experiment (i)-(iv) and the measured parameters (a)-(f) are described in Protocol 1. The optimal FCCP/CCCP concentration to induce maximal respiration should be determined for each experimental setting (details in Protocol 1), and it is advisable to also assess maximal respiratory capacity in the absence of oligomycin. The addition of pharmacological compounds or fuel substrates prior to oligomycin (not shown here) can capture further detail regarding the OCR. Rot, Rotenone; AA, Antimycin A; Oligo, Oligomycin. * Respiration in (b) is predominantly driven by proton leak, but also by substrate oxidation.*

5.2.1. Experimental set-up

Conventional Clark-type oxygen electrode chambers (e.g. Hansatech Oxygraph), which can measure oxygen (O_2) in large numbers of cells, isolated mitochondria or tissue homogenates in suspension (Barrientos et al., 2009), have been replaced more recently by cell respirometers, which perfuse buffer over live, attached cells within a sealed chamber, a set-up more suitable for use with primary neurons (Jekabsons and Nicholls, 2004, Clerc and Polster, 2012). Chambers mounted on fluorescence microscopes allow simultaneous measurement of other fluorescent indicators (Jekabsons and Nicholls, 2004). The multi-well plate reader from Agilent Technologies (Seahorse XF Flux Analyser)

can simultaneously measure both the OCR and the extracellular acidification rate (ECAR; a read-out that allows calculation of lactate release under certain conditions and therefore the rate of anaerobic glycolysis - more details are provided at the end of Section 5.2.2), although experiments are expensive and limited to non-perfused cell population measurements (Zhang and Trushina, 2017). The Oroboros Oxygraph-2k system (O2k; Oroboros Instruments) can measure O_2 consumption in cell suspensions simultaneously to other parameters such as the mitochondrial membrane potential or the ADP-ATP exchange rate mediated by the adenine nucleotide translocator (ANT) (Chinopoulos et al., 2014), but it is labour intensive and low-throughput. An overview of these two commercial systems is provided in (Horan et al., 2012). Luxcel Bioscience's MitoXpress® Xtra plate-reader assay allows population-level O_2 measurements to be multiplexed with other reporters, such as indicators of cell viability (Will et al., 2006).

Regardless of equipment, the OCR is generally inferred by measuring the levels of dissolved O_2 in the chamber/well over time, using polarographic O_2-sensing electrodes or fluorescent/phosphorescent reporters. The Seahorse system, for instance, utilises solid-state fluorescence-based sensors to measure extracellular O_2 levels within a sealed chamber for 2-6 minutes. The chamber is then unsealed (allowing the O_2 to re-equilibrate to atmospheric levels) and re-sealed to repeat the measurement. Intracellular O_2-sensing probes include nanoparticles based on the phosphorescent dye Pt(II)-tetrakis(pentafluorophenyl)porphine (PtTFPP; MitoXpress®-Intra, Luxcel Biosciences), which require phosphorescence lifetime measurements and can be detected at single-cell level or on plate readers with time-resolved fluorescence/phosphorescence detection. This probe can provide quantitative intracellular O_2 measurements in neurons and brain slices (Dmitriev et al., 2015, Kondrashina et al., 2015).

5.2.2. Experimental protocol

We here describe the most commonly deployed experimental protocol to thoroughly investigate mitochondrial bioenergetic function by measuring the OCR in intact primary neurons (

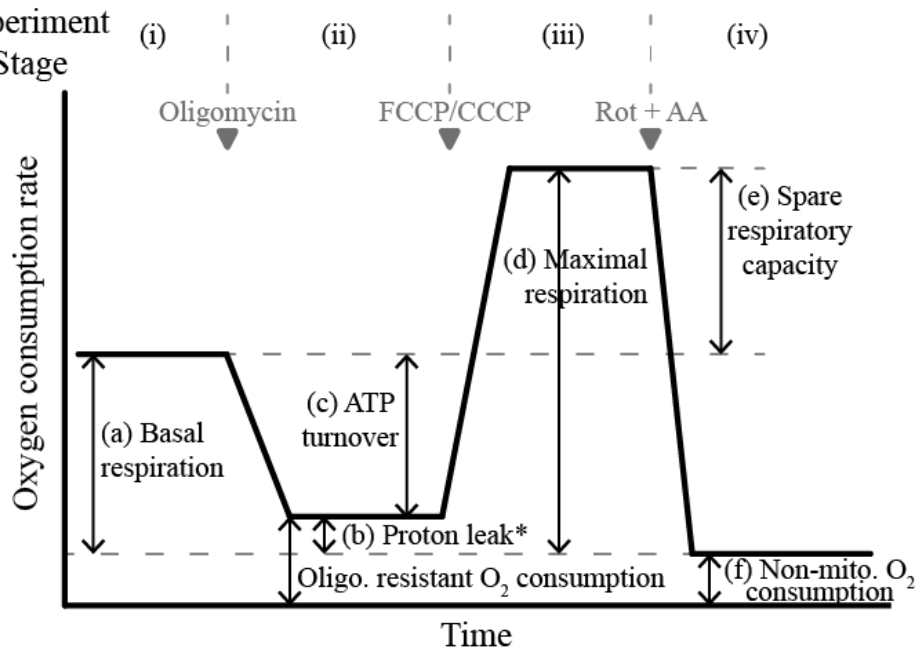

Figure 2 and Protocol 1). This protocol can be followed independently of the measurement technique.

Protocol 1: Investigating mitochondrial function in primary mouse cortical neurons by measuring the oxygen consumption rate in the presence of various inhibitors of the mitochondrial respiratory chain.

- *Primary cortical neurons preparation and culture*
  - Prepare cortical neurons from post-natal (day 0-1) or embryonic (day 16-18) mice of either sex (Hilgenberg and Smith, 2007, Sciarretta and Minichiello, 2010).
  - Seed neurons at appropriate density on pre-washed, poly-D-lysine (and/or laminin)-coated dishes suitable for OCR measurements (e.g. 100,000-300,000 cortical neurons/well in 24-well Seahorse cell culture microplates if using Seahorse XF Flux Analyser).
  - Culture neurons in appropriate media. Neurobasal medium 21103-049 is commonly used, supplemented with 0.5 mM L-glutamine and 2 % B27. It should be noted that this media contains supraphysiological glucose levels (25 mM).
  - Perform experiments after at least 8 days *in vitro.*
- *Performing the experiment*
  - Exchange culture media for appropriate 'experimental buffer' (wash neurons once to ensure complete exchange). Example buffer composition (in mM): 120 NaCl, 3.5 KCl, 0.4 KH_2PO_4, 5 $NaHCO_3$, 20 HEPES, 1.2 Na_2SO_4, pH 7.4 (NaOH), supplemented with 1.2 $CaCl_2$, 1-2 $MgCl_2$ and desired substrate (e.g. 2.5-5 mM glucose). Equilibrate cells for 1 h at 37 °C with no CO_2.
  - Different components of the proton circuit exert varied control over mitochondrial O_2 consumption. Sequential addition of specific mitochondrial inhibitors isolates these components. Such an experiment involves several stages ((i) – (iv); refer to

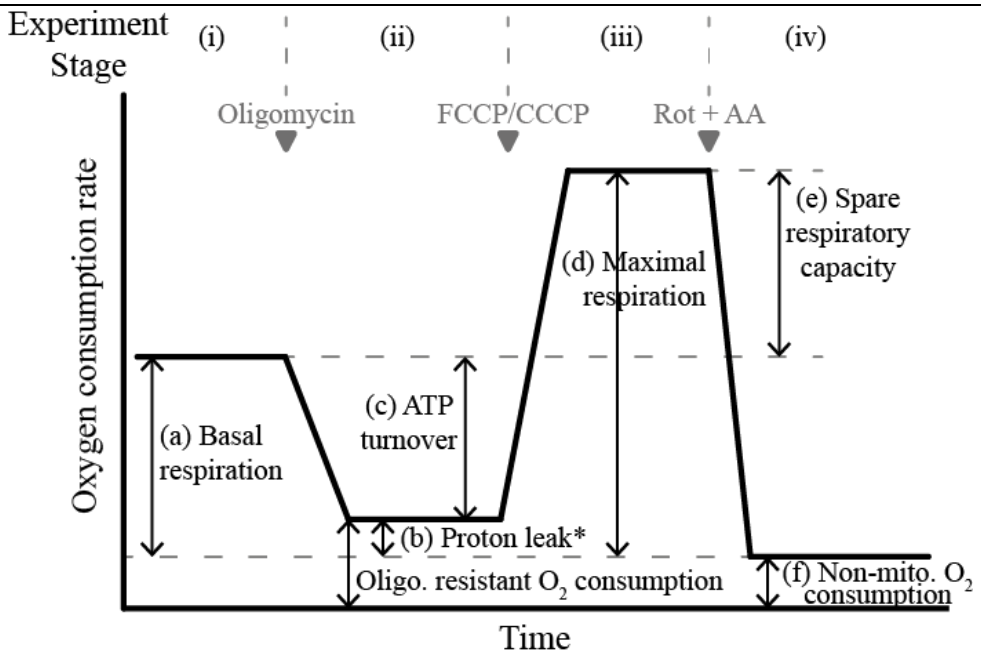

- Figure 2):
- (i) The initial OCR is a measure of mitochondrial (a) and non-mitochondrial (f) O_2 consumption, and is predominantly driven by ATP turnover (proton flow through the F_1F_o ATP synthase), and to a lesser extent by proton leak and substrate oxidation (activity of the respiratory complexes). Differences in basal O_2 consumption (in the same cellular microenvironments) can suggest; 1) altered ATP consumption, 2) altered ATP synthesis (F_1F_o ATP synthase activity), 3) disrupted transport of adenine nucleotides (ANT) or phosphate between matrix and cytoplasm, 4) altered synthesis or consumption of reducing equivalents within the matrix by substrate oxidation or the respiratory chain, respectively, 5) disrupted substrate supply to the matrix, or 6) disrupted non-mitochondrial O_2 consumption. Measurement of the additional parameters below can further elucidate the contributing factors.
- (ii) Inhibiting the F_1F_o ATP synthase with oligomycin allows the measurement of oligomycin-sensitive respiration driven by ATP turnover. Following oligomycin addition, the remaining mitochondrial O_2 consumption is predominantly controlled by the proton leak across the inner membrane, and to a lesser extent by substrate oxidation. As proton leak itself is voltage-dependent and oligomycin generally hyperpolarises mitochondria, these measurements will tend to over/underestimate the contribution of the proton leak/ATP turnover, respectively, to O_2 consumption. Such errors may significantly impact findings if comparing systems with only subtle differences between them (Brand and Nicholls, 2011, Dranka et al., 2011). Differences in the oligomycin-resistant respiration rate can indicate; 1) disrupted proton leak (accompanied by mitochondrial membrane depolarisation), 2) altered substrate oxidation (accompanied by mitochondrial membrane hyperpolarisation), or 3) disrupted non-mitochondrial O_2 consumption.
- (iii) Addition of an uncoupler (such as FCCP, CCCP or DNP) creates a proton short-circuit across the mitochondrial inner membrane, decreasing the proton-motive force and allowing respiration to increase. In this state, substrate oxidation is the dominant controller of O_2 consumption. This is considered to be maximal respiratory capacity, although this measurement critically depends on the concentration of the uncoupler.

Excess uncoupler can inhibit respiration and collapse the proton-motive force, disrupting transport processes facilitated by $\Delta\psi_m$ (e.g. the malate/aspartate shuttle, Ca^{2+} transport) or ΔpH (uptake of several metabolites). Cell density and buffer composition can also affect the concentration required to induce maximal respiration (albumin, for instance, can sequester FCCP). Vitally, therefore, the uncoupler concentration should be optimised for each experimental set-up – adding just enough to stimulate uncontrolled respiration while limiting any decrease in $\Delta\psi_m$ (**Error! Reference source not found.**; (Brand and Nicholls, 2011)). Discrepancies in maximal respiratory capacity can indicate dysfunction in the respiratory complexes, or in mitochondrial substrate uptake/supply (processes upstream of the respiratory chain) if measured in intact cells. Be aware that cellular function relies heavily on adequate mitochondrial ATP production, and that the switch to glycolysis on addition of oligomycin can induce energy failure to such an extent that, regardless of uncoupler concentration, subsequent respiration levels are not an accurate measure of maximum respiratory capacity (Ruas et al., 2016). It is therefore advisable to also assess maximal respiratory capacity in the absence of oligomycin.

- (iv) Finally, inhibition of the respiratory complexes (commonly rotenone + antimycin A to inhibit complexes I and III, respectively, although antimycin A is likely sufficient (Dranka et al., 2011)) measures O_2 consumption driven by non-mitochondrial processes, such as cytoplasmic NAD(P)H oxidases.
- The addition of pharmacological compounds or fuel substrates prior to oligomycin can capture further detail (Dranka et al., 2011). Compounds to induce varying degrees of neuronal stimulation, such as gramicidin (permeabilises plasma membrane), carbachol (acetylcholine receptor antagonist), or veratridine (inhibitor of Na^+ channel inactivation) (Llorente-Folch et al., 2013), increase ATP demand and introduce a 'second hit' that may be required to unveil underlying deficiencies not apparent in the basal, resting state. Addition of alternative fuel substrates such as lipids or amino acids can help to investigate fuel dependence and metabolic flexibility.

- *Experiment analysis*
  - Measurement of the OCR in this way allows calculation of several experimental parameters ((a) – (f) in

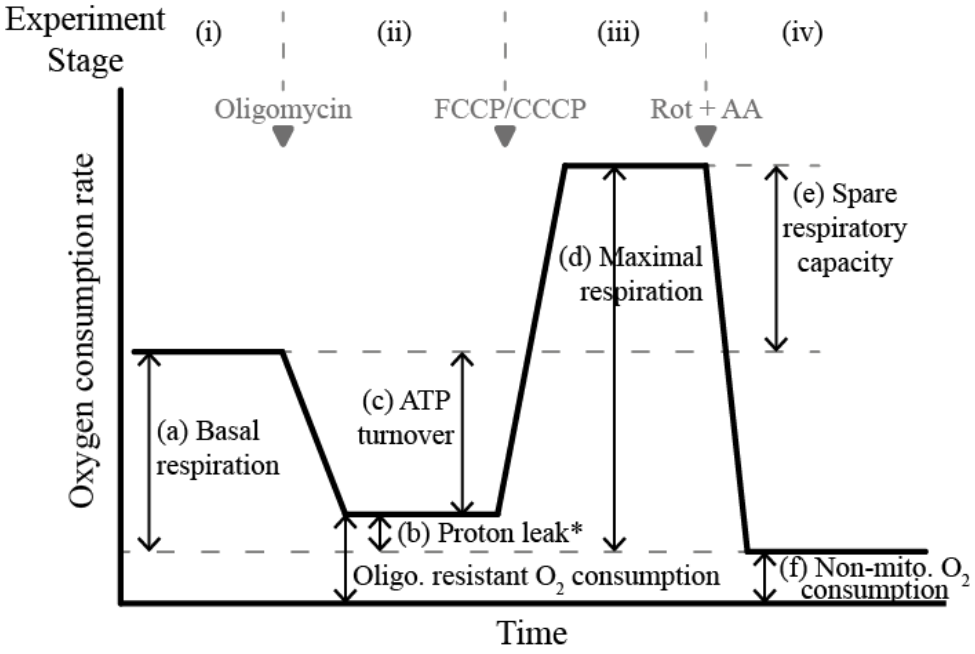

- Figure 2), detailed below.
- The average OCR during stage (iv), non-mitochondrial O_2 consumption (f), is subtracted from the average OCR during all other stages to determine 'basal respiration' (a), 'proton leak' (b), and 'maximal respiration' (d). Subtraction of non-mitochondrial O_2 consumption also removes any background signal (Clerc and Polster, 2012).
- ATP turnover, assessed as oligomycin-sensitive respiration (c), is calculated as (a) – (b).
- Spare respiratory capacity (e), also known as respiratory reserve, is calculated as (d) – (a), and is a measure of the cell's ability to respond to an increase in energy demand.
- The calculation of ratios from these parameters can be informative, and provides a form of internal normalisation. The *coupling efficiency* between ATP turnover and basal respiration is calculated as (c)/(a). The *cell respiratory control ratio* (RCR; similar but not identical to the RCR measured in isolated mitochondria) is calculated as (d)/(b) (Brand and Nicholls, 2011). A higher RCR generally indicates more coupled mitochondria and more efficient ATP synthesis (Clerc and Polster, 2012). The *bioenergetic health index* is calculated as (c*e)/(b*f) (Chacko et al., 2014).
- Further guidelines for interpretation of OCR measurements can be found in (Brand and Nicholls, 2011, Mookerjee et al., 2017, Dranka et al., 2011).

- *Data analysis*
  - The measured OCR ([O_2]/time) can be normalised to cell number, total protein content or to levels of specific proteins of interest, giving final units of [O_2]/time/cell number, [O_2]/time/μg protein or [O_2]/time/band density (Dranka et al., 2011, Salabei et al., 2014). The OCR can also be normalised to the activity of citrate synthase, a mitochondrial matrix TCA cycle enzyme commonly assumed to be a measure of mitochondrial abundance (Rhein et al., 2009, Barrientos et al., 2009, Spinazzi et al., 2012).
  - Changes in cell viability, mitochondrial density, or protein levels will impact the normalised OCR, and should be reported. In experiments where neurons are exposed to toxic manipulations (e.g. glutamate), it may be particularly important to normalise the OCR to cell viability throughout the experiment (Jekabsons and Nicholls, 2004).
  - As a guideline for multi-well experiments (e.g. for Seahorse measurements), a minimum of 3 individual wells per condition should be included per plate, with experiments repeated in 3 independent cultures. Variability between wells and cultures may necessitate increased replicates to identify small effects.
  - One-way analysis of variance with repeated measures can be used to test for differences between OCR measurements at specific time-points.

For thorough investigation of the cellular metabolic state and bioenergetic capacity, OCR measurements can be coupled with those of the extracellular acidification rate (ECAR). While lactate release (specifically, protons co-transported with lactate) contributes to ECAR, CO_2 formation from mitochondrial oxidative decarboxylation and the oxidative pentose phosphate pathway also contributes. OCR and ECAR measurements can be combined to calculate lactate release under certain conditions (the buffering power of the media must be calculated) (Mookerjee et al., 2015, Mookerjee et al., 2016, Mookerjee et al., 2017), but it should be noted that, even after correction, ECAR only determines anaerobic glycolysis (i.e. the portion of pyruvate metabolised to lactate), whereas the true rate of glycolysis (glucose metabolised to pyruvate) would also include pyruvate metabolised to

Acetyl CoA. Algorithms are also available that utilise OCR and ECAR measurements to accurately calculate mitochondrial and cytosolic ATP production and consumption, providing information on the cellular bioenergetic state, capacity and flexibility (Mookerjee et al., 2015, Mookerjee et al., 2016, Mookerjee et al., 2017).

5.3. Mitochondrial membrane potential

The mitochondrial membrane potential ($\Delta\psi_m$), defined as the difference in electrical potential between the mitochondrial matrix and the cytosol, is commonly considered as a semi-quantitative read-out for the full proton-motive force (Δp), as $\Delta\psi_m$ dominates over ΔpH_m (Nicholls and Ferguson, 2013) (although changes in ΔpH_m do not necessarily parallel with $\Delta\psi_m$, (Perry et al., 2011)). While $\Delta\psi_m$ and ΔpH_m both contribute to the regulation of ATP synthesis by Δp, $\Delta\psi_m$ alone provides the charge gradient to regulate the transport of Ca^{2+} and other ions across the mitochondrial membrane (Perry et al., 2011). It is important to note that $\Delta\psi_m$ is not necessarily a good indicator of mitochondrial health, as ATP-synthesising mitochondria can have a reduced $\Delta\psi_m$ to those with ATP synthase switched off. These measurements should therefore be interpreted together with measurements of OCR or NAD(P)H. Small fluctuations in $\Delta\psi_m$ can indicate disrupted respiration, ATP synthesis, or ionic fluxes across the mitochondrial membrane (Nicholls and Budd, 2000, Nicholls, 2006, Ward et al., 2007). Marked $\Delta\psi_m$ depolarisation is generally correlated with neuronal death, and may indicate mitochondrial outer membrane permeabilisation during apoptosis or mitochondrial permeability transition during ROS or Ca^{2+}-mediated injury. In response to oligomycin, $\Delta\psi_m$ hyperpolarisation indicates that mitochondria were still generating ATP prior to drug exposure (ATP synthase operating in forward mode), while immediate depolarisation indicates that mitochondria had been net ATP consumers (ATP synthase reversal, where glycolytic ATP maintains $\Delta\psi_m$) (Ward et al., 2000, Nicholls and Budd, 2000). If depolarisation is preceded by a lag phase, it is likely that oligomycin caused secondary mitochondrial dysfunction, often due to mitochondrial Ca^{2+} overload followed by opening of the permeability transition pore (Irwin et al., 2003). Although it is a less sensitive measure than the OCR, the magnitude and direction of $\Delta\psi_m$ fluctuations can provide complementary information to OCR experiments (Brand and Nicholls, 2011). The cause of changes in the

oligomycin-resistant mitochondrial OCR (

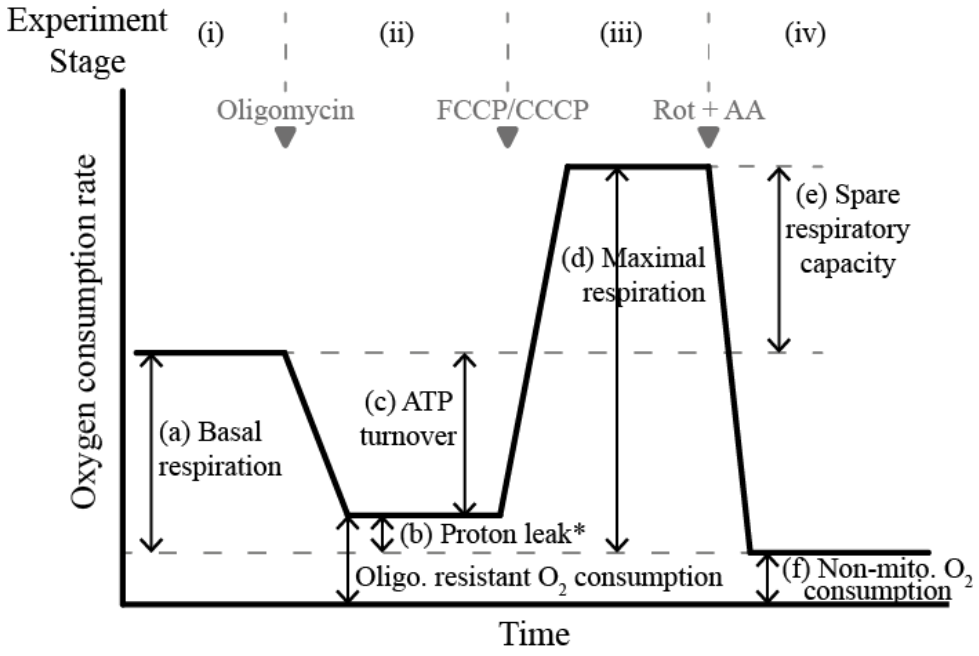

Figure 2, (b)), for instance, can be further investigated by measuring $\Delta\psi_m$ – an increased H^+ leak would decrease $\Delta\psi_m$, while increased substrate oxidation increases $\Delta\psi_m$. High concentrations of a mitochondrial uncoupler that collapse $\Delta\psi_m$ (**Error! Reference source not found.**) are commonly added at the end of an experiment as a control for signal specificity.

5.3.1. Experimental set-up

$\Delta\psi_m$ is commonly measured using membrane-permeant, lipophilic, cationic fluorescent probes which accumulate in the negatively charged mitochondrial matrix in proportion to $\Delta\psi_m$. The magnitude of accumulation is described by the Nernst equation (Nicholls and Ferguson, 2013), but can be affected by mitochondrial binding of the probe (Perry et al., 2011). The fluorescent signal can be measured by flow-cytometry or microplate photometers for fixed end-point or population level analyses, respectively. Time-lapse fluorescence imaging in single living cells allows the measurement of intrinsic cell-to-cell heterogeneity and has been applied extensively in the investigation of neuronal metabolism (Connolly and Prehn, 2015). $\Delta\psi_m$ can also be monitored in conjunction with other fluorescent reporters to obtain simultaneous measurements of multiple cellular parameters.

All probes are substrates of the multidrug resistance (MDR) transporters. Primary neurons do not generally express these transporters, but they are often over-expressed in cultured cell lines and may limit mitochondrial loading. Cyclosporin A, an inhibitor of the permeability transition pore (PTP), also inhibits MDR transporters, leading to increased mitochondrial probe loading and confounding studies investigating the contribution of the PTP to mitochondrial depolarisation (Bernardi et al.,

2001). This issue can be overcome by using Cyclosporin H, which inhibits MDR transporters but not the PTP.

Tetramethylrhodamine methyl ester (TMRM; Molecular Probes) is one of the most commonly used fluorescent reporters of $\Delta\psi_m$ and is less toxic than TMRE and Rh123 (Scaduto and Grotyohann, 1999). TMRM can be excited on epi-fluorescence, confocal, or 2-photon microscopes. 2-photon imaging on the single mitochondrial level can reduce photo-toxicity and photo-bleaching compared to confocal microscopy (Hayakawa et al., 2005). TMRM is predominantly utilised as a single-excitation, single emission dye, and is therefore affected by focus drift, laser intensity fluctuations, photobleaching or changes in cell/mitochondrial volume. Appropriate light control experiments to ensure signal stability are therefore crucial (for a dual-excitation approach in isolated mitochondria, see (Scaduto and Grotyohann, 1999)). Without calibration, TMRM provides a qualitative measure of $\Delta\psi_m$. The kinetics of the TMRM signal depend on the relatively slow equilibration of the probe across the plasma membrane (addition of tetraphenylboron can increase the rate of diffusion across membranes (Ward et al., 2000)), and the contribution of the plasma membrane potential ($\Delta\psi_p$) to the TMRM signal (or, indeed, to any cationic probe) cannot be discounted (Ward et al., 2000, Nicholls and Budd, 2000, Perry et al., 2011). To overcome this issue, $\Delta\psi_p$ must be monitored in parallel with $\Delta\psi_m$, using fluorescent anionic probes such as $DiBAC_4(3)$ (ThermoFisher) or a component of the Membrane Potential Assay Kit from Molecular Devices (commonly termed plasma membrane potential indicator, PMPI) (Nicholls, 2006). Starting from inferred initial values, relative $\Delta\psi_m$ and $\Delta\psi_p$ values can subsequently be calculated using the Nernst equation in Excel (Ward et al., 2000, Nicholls, 2006) or MATLAB (Ward et al., 2007). Absolute quantification can be achieved using mathematical models (Gerencser et al., 2012), although issues such as dye extrusion from the cell should be considered.

The concentration of TMRM (and other fluorescent cationic probes) is an important consideration in experimental design, and can be classified as either 'quench' or 'non-quench' mode. High concentrations are classified as 'quench' mode, where densely packed TMRM molecules within the mitochondrial matrix are quenched. A transient increase in the whole-cell TMRM signal in this instance therefore indicates $\Delta\psi_m$ depolarisation – the quenched probe leaves the matrix and is unquenched, leading to a transiently brighter cellular signal until the probe more slowly re-equilibrates with the extracellular space. In contrast, TMRM in 'non-quench' mode (<~30 nM) remains fluorescent within the mitochondrial matrix, and $\Delta\psi_m$ depolarisation leads to a decrease in the fluorescent signal. Non-quench mode is preferable to more reliably estimate slower changes in potential and to compare $\Delta\psi_m$ between populations, as the number of TMRM molecules and their fluorescence are roughly linearly related (Nicholls, 2006, Brand and Nicholls, 2011, Perry et al., 2011). Lower dye concentrations are also more tolerable, and reduce the dye's impact on mitochondrial function (Scaduto and Grotyohann, 1999). However, the TMRM signal in non-quench

mode does not distinguish between mitochondrial and plasma membrane potential (see earlier) (Brand and Nicholls, 2011). The precise TMRM concentrations for quench or non-quench mode can be determined using FCCP – in quench mode, addition of ~10 μM FCCP (to collapse $\Delta\psi_m$) induces a transient spike in TMRM fluorescence that is absent in non-quench mode (Brand and Nicholls, 2011, Nicholls, 2006). It must be emphasised that this transient response means that quench mode must not be used in flow-cytometry or to compare two cell populations.

TMRE (tetramethylrhodamine ethyl ester) and rhodamine 123 (Rh123; Molecular Probes) are other cationic fluorescent dyes that can be used to report changes in $\Delta\psi_m$, although these dyes may bind to the mitochondrial membrane and affect mitochondrial respiration to a greater extent than TMRM (Scaduto and Grotyohann, 1999). Rh123 only slowly crosses the plasma membrane and is therefore less affected by $\Delta\psi_p$ over short timescales. Rh123 is therefore commonly used in short-term experiments (minutes) where 'quench' mode is desired, such as when rapid step changes in $\Delta\psi_m$ are expected (Nicholls, 2006, Perry et al., 2011). In these instances, Rh123 should be removed from the media and cells washed before imaging (Hayakawa et al., 2005, Ward et al., 2000). Mitotracker dyes are not suitable to monitor $\Delta\psi_m$ as mitochondrial binding prevents probe redistribution (Bernardi et al., 2001). The use of $DiOC_6$ or JC-1 should also be avoided, due to high toxicity, sensitivity to loading concentration, and $\Delta\psi_m$-independent fluorescence changes (Perry et al., 2011). Practical guides on the use of cationic fluorescent probes to monitor $\Delta\psi_m$ are provided in (Joshi and Bakowska, 2011, Perry et al., 2011).

5.3.2. Experimental protocol

In Protocol 2, we provide experimental guidelines to monitor changes in mitochondrial membrane potential in primary cortical neurons exposed to mitochondrial respiratory chain inhibitors. Many of the steps in this protocol can be generalised to other similar experiments.

Protocol 2: Utilising live-cell fluorescence microscopy to monitor changes in mitochondrial membrane potential (by TMRM) in primary mouse cortical neurons exposed to mitochondrial respiratory chain inhibitors.

- *Primary cortical neurons preparation and culture*
  - Prepare cortical neurons from post-natal (day 0-1) or embryonic (day 16-18) mice of either sex (Hilgenberg and Smith, 2007, Sciarretta and Minichiello, 2010).
  - Seed neurons at appropriate density on pre-washed, poly-D-lysine-coated dishes suitable for microscopy (e.g. 1-2x10^5 cortical neurons/cm^2 in 12 or 22 mm aperture glass-bottomed WillCo dishes (WillCo Wells)).
  - Culture neurons in appropriate media e.g. Neurobasal medium 21103-049 supplemented with 0.5 mM L-glutamine and 2 % B27. It should be noted that this media contains

supraphysiological glucose levels (25 mM).
    - Perform experiments after at least 8 days *in vitro*.
- *Imaging set-up*
    - On a confocal microscope, TMRM can be excited with a 543 Helium-Neon (HeNe) excitation laser (3-5 % of 1 mW), or similar illumination (peak excitation ~550 nm). Its peak emission is ~576 nm and can be detected using e.g. a 560 nm long-pass filter.
    - On a 2-photon microscope, TMRM can be excited at ~830 nm (Hayakawa et al., 2005).
    - Dichroic beam splitters and filter wheels in the excitation and emission light path, containing filter sets appropriate for TMRM wavelengths, are required.
    - Efforts should be made to reduce phototoxicity – minimise laser excitation power, exposure time and imaging frequency. Photobleaching can decrease the fluorescent signal and phototoxicity leads to excessive neuronal death. Appropriate vehicle controls are necessary to control for effects of phototoxicity on fluorescence.
    - Experiments should be performed at 37 °C, as lower temperatures may alter the TMRM equilibration kinetics and/or neuronal physiology. This requires a temperature controlled microscope stage, chamber and/or objective lens.
    - Imaging set-up (laser and filter settings, imaging frequency etc.) should remain as similar as possible between experiments, to allow inter-experiment comparison.
- *Preparing the cells*
    - Exchange culture media for appropriate experimental buffer including 10 nM TMRM (non-quench mode; wash neurons once to ensure complete exchange). Example buffer composition (in mM): 120 NaCl, 3.5 KCl, 0.4 KH_2PO_4, 5 $NaHCO_3$, 20 HEPES, 1.2 Na_2SO_4, pH 7.4 (NaOH), supplemented with 1.2 $CaCl_2$, 1-2 $MgCl_2$ and desired substrate (e.g. 2.5-5 mM glucose).
    - Equilibrate neurons in TMRM for 45-60 min prior to imaging (at 37 °C in the dark, no CO_2 if using experimental buffer). Baseline recording prior to drug addition can verify dye equilibration.
    - The buffer surface can be covered with mineral oil, or the chamber closed, to minimise evaporation during experiments.
    - TMRM should be kept in the buffer throughout the experiment, as removal will cause re-equilibration of the probe across the plasma and mitochondrial membranes, altering the fluorescent signal (see (Perry et al., 2011) for potential issues with dye equilibration). In contrast to cancer-derived cell lines, the addition of Cyclosporin H or verapamil (to inhibit the rhodamine-sensitive MDR transporters) is generally not required in primary neurons.
- *Performing the experiment*
    - Mount chamber/culture dish on microscope stage.
    - Record baseline fluorescence (usually for ~10 min) to ensure signal stability prior to treatment.
    - Image acquisition at 1 min intervals should be acceptable for relatively short-term experiments (< 2 h) on an epifluorescence or confocal microscope, dependent on the specific imaging set-up.
    - In the absence of a suitable perfusion system, pharmacological compounds can be added directly to the buffer on stage. Compounds can be pre-prepared in experimental buffer (+TMRM) for ease of mixing.

- *Testing respiratory complex activity (Figure 3)*
  - Suggested drug concentrations are listed in **Error! Reference source not found.**. Drugs can be added alone or in combination.

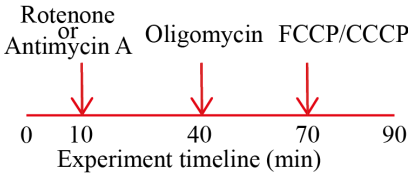

  - Rotenone and antimycin A inhibit Complex I and Complex III, respectively. In healthy respiring neurons, this inhibits respiration and partially depolarises the mitochondrial membrane (TMRM signal decreases in non-quench mode).
  - Oligomycin inhibits ATP synthase. This may depolarise/hyperpolarise the mitochondrial membrane (decrease/increase TMRM signal in non-quench mode), depending on the prior direction of ATP synthase operation (ATP producing or consuming, respectively) (Ward et al., 2000, Nicholls and Budd, 2000).
  - The addition of high concentrations of FCCP (10 μM) at the end of the experiment should rapidly collapse $\Delta\psi_m$ (and TMRM signal) indicating that the TMRM signal during the experiment emanated from mitochondria. Such high concentrations also more slowly depolarise the plasma membrane (Nicholls, 2006).
  - Vehicle and light control experiments should also be performed.
  - Sufficient time should be allowed between drug additions for the TMRM signal to stabilise (up to 30 min).
  - Compounds can also be added as in the standard OCR experiment (to complement these measurements) (Protocol 1).
- *Image processing and analysis*
  - Image processing can be performed using tools such as MetaMorph (Molecular Images) or the open-source ImageJ (https://imagej.nih.gov/ij/).
  - Subtract background signal, identify regions of interest (ROI; e.g. individual cells, or mitochondrial-enriched regions), and measure the (thresholded) average signal intensity within the ROI. The total fluorescence within the cell soma can be measured, assuming mitochondria within the cell respond similarly (relatively homogenous response throughout) (Perry et al., 2011), and provided that mitochondrial loading of the probe has been verified.

For each ROI, plot the signal intensity over time (absolute signal intensity, or signal intensity

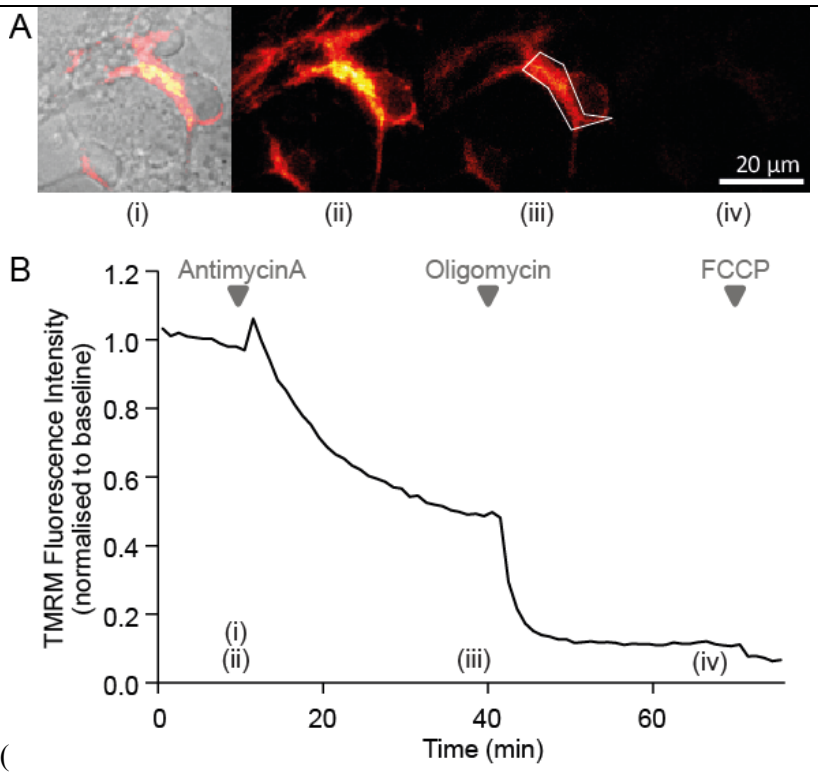

normalised to baseline signal) (

- Figure 3).

- *Data analysis*
  - As a guideline when investigating single-cell behaviour, at least 25 cells from 3 independent cultures should be analysed, although variability between cells and cultures may necessitate increased replicates to identify small effects. Required cell numbers can be calculated based on the expected effect size and desired power.
  - The response of each neuron can be treated as an independent event in statistical analyses, unless culture-to-culture variability is higher than cell-to-cell variability within cultures.
  - One-way analysis of variance with correction for repeated measures can be used to test for differences between TMRM measurements at specific time-points.
  - As discussed in the main text, the contribution of $\Delta\psi_p$ to the TMRM signal can be determined by simultaneous use of a $\Delta\psi_p$-sensitive probe, allowing relative or absolute quantification of $\Delta\psi_m$ (Ward et al., 2000, Ward et al., 2007, Gerencser et al., 2012, Nicholls, 2006).

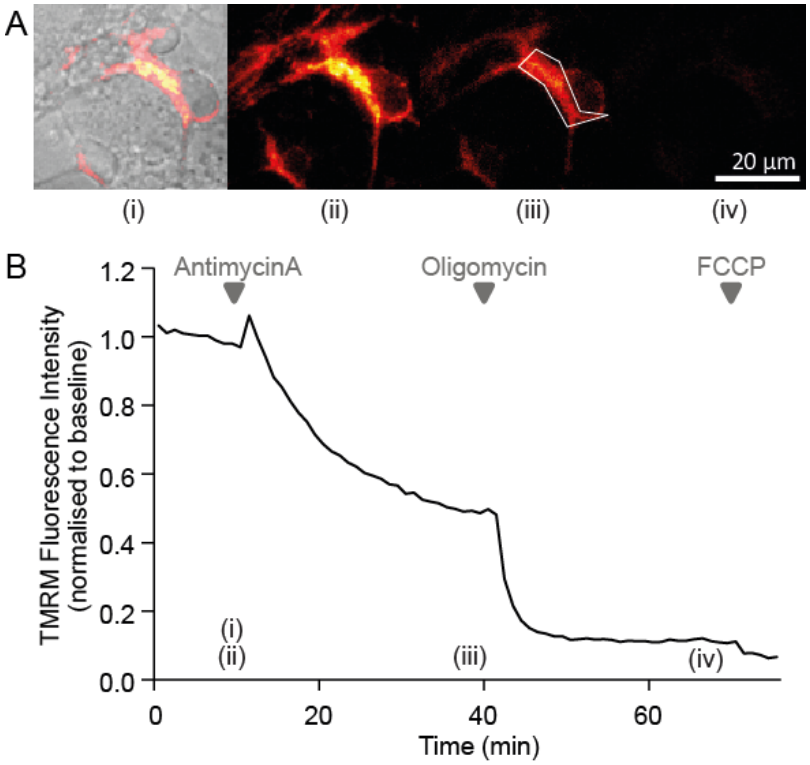

Figure 3: Representative images and time-series data from TMRM (10 nM) measurements in wild-type mouse cortical neurons exposed to mitochondrial inhibitors. (A) Brightfield and TMRM fluorescence images were captured on a Zeiss Axiovert 100 microscope (brightfield and TMRM fluorescence are merged in the left-most image, TMRM only in the other images). (B) Time-series TMRM fluorescence measurements within the region of interest marked by the white polygon in (A)(ii). The precise time-points of the images in (A) are marked (i)-(iii) on the graph. Baseline fluorescence was recorded for 10 min pre-treatment and used to normalise the signal. Complex III inhibition with antimycin A (1 µM) induced a decrease in TMRM fluorescence, indicating mitochondrial membrane depolarisation. Subsequent oligomycin addition (2 µg/ml) further reduced TMRM fluorescence, indicating that prior to oligomycin addition the mitochondrial membrane potential was being maintained by the F_1F_o ATP synthase operating in reverse. The loss of any remaining TMRM fluorescence after FCCP addition (10 µM) indicates mitochondrial membrane potential collapse.

5.4. Mitochondrial NAD(P)H

Pyridine nucleotides are electron-shuttling agents that act as co-factors in enzymatic reduction-oxidation (redox) reactions. Nicotinamide adenine dinucleotides (NAD^+/NADH and the phosphorylated $NADP^+$/NADPH) are pyridine nucleotides that play a central role in mitochondrial energy metabolism and in the maintenance of redox status. In neurons, NADH is the principal electron donor in the respiratory chain, and is oxidised from NADH to NAD^+ at complex I to drive mitochondrial OxPhos (Shuttleworth, 2010). Mitochondrial NADH is maintained by the reduction of NAD^+ to NADH in the TCA cycle and via the import of NADH-derived reducing equivalents driven by the malate/aspartate shuttle. NAD^+ can also be consumed by Poly (ADP-ribose) polymerase (PARP) isozymes and sirtuins (Kahraman et al., 2015, Fang et al., 2016). $NADP^+$/NADPH does not contribute directly to mitochondrial OxPhos, but primarily supports the maintenance of reduced glutathione (GSH) and thioredoxin pools (Lewis et al., 2014). NADPH is maintained by the activity of the NADP-isocitrate dehydrogenase (ICDH) and the NADP-malic enzyme, though the mitochondrial $NADP^+$/NADPH pool is often assumed to be largely reduced and invariant compared to the mitochondrial NAD^+/NADH pool (Nicholls and Budd, 2000). Electrons from NADH and NADPH (termed NAD(P)H here) reactions can also be transferred to oxygen molecules (e.g. by NADPH oxidases) to generate reactive oxygen species in the form of superoxide (Blacker and Duchen, 2016). Measurement of mitochondrial NAD(P)H can be most informative when linked to $\Delta\psi_m$ measurements, as processes regulating both parameters are tightly linked (Brand and Nicholls, 2011). A decrease in mitochondrial NAD(P)H can indicate enhanced respiratory chain activity (increased NADH oxidation), reduced TCA cycle activity (decreased NAD^+ reduction), or increased NAD^+ consumption.

5.4.1. Experimental set-up

NAD(P)H can be monitored by measuring endogenous autofluorescence, through the use of genetically-encoded fluorescent proteins, or by high performance liquid chromatography, labelled spectrometry techniques, or commercially available enzymatic assays (e.g. Promega's NAD/NADH-Glo™ Assay).

Autofluorescence

Both NADH and NADPH autofluoresce in their reduced, but not in their oxidised state, and produce spectrally identical autofluorescence (Chance, 1962). The cellular NAD(P)H autofluorescence intensity is considered to be dominated by protein-bound mitochondrial NAD(P)H, as the autofluorescence signal co-localises with mitochondrial markers, and NAD(P)H autofluorescence intensity is enhanced when the nucleotides are protein-bound and 'active' (Shuttleworth, 2010, Ogikubo et al., 2011).

NAD(P)H autofluorescence can be detected using epifluorescent illumination or confocal microscopes equipped with UV lasers. It is excited by near ultraviolet wavelength light (340-360 nm), and emission is detected at ~450 nm (excitation/emission spectra similar to Hoechst) (Chance, 1962). Low excitation wavelengths are required to distinguish NAD(P)H from flavoprotein autofluorescence (which has an excitation peak ~450 nm). While autofluorescence detection is a non-invasive approach, excessive exposure of cells to UV wavelength excitation can be highly phototoxic, and efforts to reduce exposure are required (e.g. optimising detection sensitivity and reducing laser intensity, pixel dwell-time, exposure time and imaging duration/frequency), sometimes resulting in detection difficulties or sub-optimal signal-to-noise levels. 2-photon microscopy (excitation peak ~710 nm; emission ~400-500 nm) has also been used in dissociated cultures (Hayakawa et al., 2005, Pardo et al., 2006) and in brain tissue slices (Kasischke et al., 2004, Shuttleworth, 2010). 2-photon NAD(P)H excitation wavelengths are phototoxic and also excite flavoprotein autofluorescence (Huang et al., 2002). Semi-quantification and comparison of mitochondrial NAD(P)H levels between experiments can be achieved by determining the autofluorescence dynamic range between maximal and minimal NADH for each sample (neglecting the contribution from NADPH), with maximal oxidation induced by an uncoupler such as FCCP, and maximal reduction induced by an effective inhibitor of respiration such as cyanide (Blacker and Duchen, 2016, Blacker et al., 2017).

Fluorescence lifetime imaging microscopy (FLIM) enables semi-quantitative measurements of free and protein-bound mitochondrial NAD(P)H and may further identify the relative contribution of NADH and NADPH to the autofluorescence signal (Blacker and Duchen, 2016). FLIM measures the pixel-by-pixel autofluorescence lifetime on a defined sample area, under 2-photon pulsed excitation, by recording the delay between the pulse and fluorescence emission (lifetime) (Chakraborty et al., 2016). NAD(P)H autofluorescence lifetimes vary based on their binding state - the lifetime of free NAD(P)H molecules (~0.4 ns) is shorter than that of the protein-bound, active molecule (~2-4 ns) (Blacker and Duchen, 2016). Since the relative amplitude of each lifetime component is proportional to its concentration, FLIM analysis can be used to measure the contribution of active NAD(P)H with respect to its free counterpart. This is particularly important in the study of respiratory chain processes in the mitochondrial compartment. The precise autofluorescence lifetime also depends on the fluorophore's local environment, and FLIM techniques may therefore provide an alternative measure of characteristics such as pH (Ogikubo et al., 2011).

5.4.2. Experimental protocol

Protocol 3: Utilising live-cell fluorescence microscopy to monitor NAD(P)H autofluorescence in primary mouse cortical neurons exposed to mitochondrial respiratory chain inhibitors.

- Prepare and culture primary cortical neurons as described in Protocol 2, performing experiments after at least 8 days *in vitro*.
- *Imaging set-up*
  - The NAD(P)H autofluorescence peak excitation wavelength (~340 nm) and peak emission wavelength (~450 nm) are similar to those of Hoechst. An epifluorescence microscope therefore requires a transmission curve that includes near UV wavelengths. On a confocal microscope, NAD(P)H autofluorescence can be excited with a UV excitation laser (364 nm Argon Gas Ion laser or 355 nm or 375 nm DPSS laser). The 2-photon excitation peak of NAD(P)H autofluorescence ~710 nm.
  - Dichroic beam splitters and filter wheels in the excitation and emission light path, containing filter sets appropriate for NAD(P)H autofluorescence, are required e.g. a 450 nm band-pass filter (30/40 nm bandwidth). It is essential to use a band-pass filter (rather than a long-pass filter) to minimise contamination of the signal by flavoprotein autofluorescence.
  - Phototoxicity is a major concern when exciting neurons at near UV wavelengths – minimise laser excitation power, exposure time, imaging frequency and imaging resolution. The use of UV filters (e.g. neutral density UV filter) can also be considered. Appropriate control experiments should be performed. See also (Blacker et al., 2017).
  - As for TMRM experiments, autofluorescence imaging should ideally be performed at 37 °C.
  - Imaging set-up (laser and filter settings, imaging frequency etc.) should remain as similar as possible between experiments, to allow inter-experiment comparison.
- *Preparing the cells*
  - Exchange culture media and equilibrate neurons as for Protocol 2 (simultaneous monitoring of TMRM is also possible).
- *Performing the experiment*
  - Neurons can be imaged as described in Protocol 2 (with settings specific to detect autofluorescence), although extra care is needed to reduce phototoxicity when exciting and detecting NAD(P)H autofluorescence, so imaging frequency and experiment duration may need to be reduced. NAD(P)H autofluorescence can equilibrate relatively rapidly (within 5 min, Figure 4) following drug addition.
- *Testing respiratory complex activity*
  - Suggested drug concentrations are listed in **Error! Reference source not found.**.
  - Oligomycin inhibits ATP synthase and thereby reduces the flux through the respiratory chain. In healthy, unimpaired neurons this decreases NADH consumption and increases autofluorescence (Figure 4).

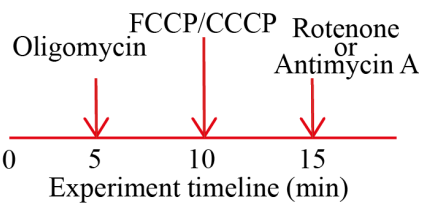

  - Mitochondria uncoupling (low concentrations of e.g. FCCP/CCCP, see Table 2) increases NADH oxidation, decreasing autofluorescence ((Blacker and Duchen, 2016), Figure 4).
  - Inhibition of respiration with rotenone or antimycin A reduces NADH oxidation and increases NAD(P)H autofluorescence (Blacker and Duchen, 2016).
  - Standard calibration of the NAD(P)H autofluorescence dynamic range is performed by inducing maximal NADH oxidation with an uncoupler (e.g. FCCP/CCCP), followed by maximal reduction induced by an inhibitor of respiration such as cyanide or antimycin A.

- Alternative substrates, modulators or compounds can be added to analyse additional aspects of NAD(P)H processing.
- Vehicle control experiments should also be performed.

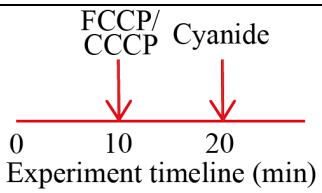

- *Image processing and analysis*
  - Perform image processing and analysis similar to that described in Protocol 2.
  - Subtract background signal from the image.
  - Identify regions of interest (ROI) for analysis. Areas of brightest autofluorescence can be considered areas of high mitochondrial density (Figure 4). Selecting a ROI within these areas minimises background signal, which can dilute the dynamic range of the autofluorescence signal.
  - Measure the average signal intensity within the ROI – for autofluorescence measurements, thresholding may reduce the signal dynamic range.
  - For each ROI, plot the signal intensity over time (absolute signal intensity, or signal intensity normalised to baseline signal) (Figure 4).
- *Data analysis*
  - Analyse the autofluorescence signal in single neurons as described in Protocol 2.

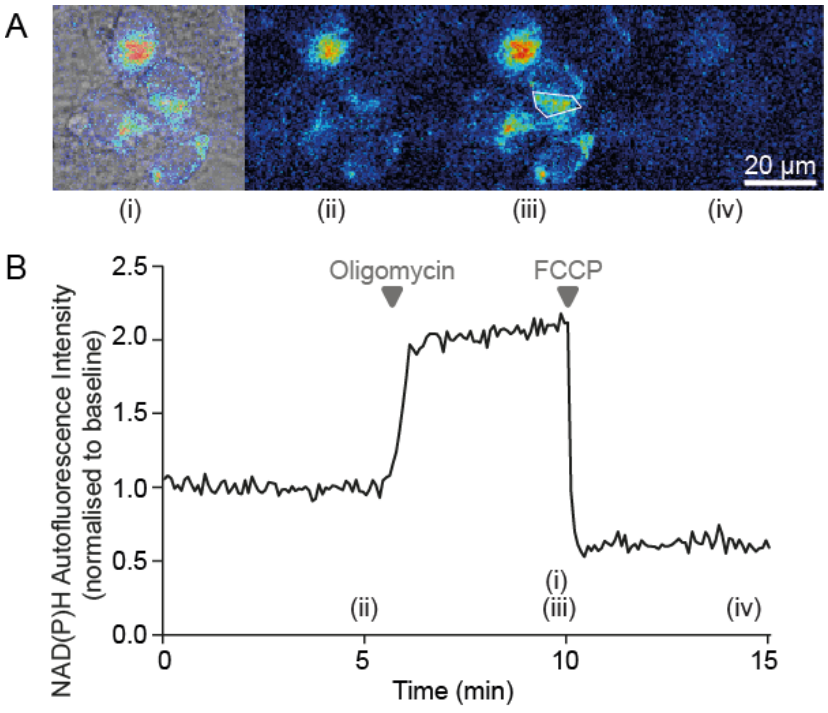

Figure 4: Representative images and time-series data from NAD(P)H autofluorescence measurements in wild-type mouse cortical neurons exposed to mitochondrial inhibitors. (A) Brightfield and NAD(P)H autofluorescence images were captured on a Zeiss Axiovert 100 microscope. (B) Time-series autofluorescence measurements from the region of interest marked within a white polygon in (A)(iii). The precise time-points of the images in (A) are marked (i)-(iv) on the graph. Baseline fluorescence was recorded for 5 min pre-treatment and used to normalise the signal. Inhibition of the F_1F_o ATP synthase with oligomycin (2 µg/ml) reduced NADH consumption by the respiratory chain,

leading to an increase in the autofluorescence signal. Subsequent mitochondrial uncoupling with FCCP (0.5 μM) increased respiratory NADH oxidation, decreasing autofluorescence.

Flavoprotein autofluorescence provides a similar, though not identical, measure of mitochondrial metabolism, and can be especially useful in the absence of available UV excitation or as a complementary measure to NAD(P)H autofluorescence. FAD^+ is reduced to $FADH_2$ in the TCA cycle, and $FADH_2$ is oxidised to FAD^+ via the activity of Complex II in the respiratory chain. As flavoproteins autofluoresce in their oxidised (FAD^+), but not in their reduced ($FADH_2$) form, signal fluctuations are expected to be inverted compared to NAD(P)H autofluorescence. The flavoprotein peak excitation wavelength is ~450 nm, while emission is detected ~510 nm (Huang et al., 2002, Shuttleworth, 2010, Chakraborty et al., 2016).

Fluorescent Reporter Proteins

Genetically-encoded fluorescent reporters and their use in biological research are introduced in Section 5.6 "Fluorescent reporters of mitochondrial ATP, calcium (Ca^{2+}) and pH". Fluorescent proteins (FPs) to measure mitochondrial NADH or NADH:NAD^+ have an improved signal to noise ratio and are less phototoxic than autofluorescence detection methods, but are slower acting, can contribute to NAD(P)H buffering, and require transfection and mitochondrial targeting (San Martin et al., 2014).

Current genetically-encoded fluorescent reporters of NADH or of the NADH:NAD^+ ratio contain the bacterial Rex protein, a transcription factor that, when bound to NADH, undergoes a conformational change (Bilan et al., 2014, Bilan and Belousov, 2016). Frex variants are dual excitation reporters of NADH, comprising a circularly permuted yellow FP (cpYFP) inserted between two Rex proteins, that have been successfully targeted to mitochondria (Frex-Mit/C3L194K) (Zhao et al., 2011b). RexYFP, comprising cpYFP inserted into a Rex homolog, is significantly smaller than Frex, and has also been successfully utilised to report the mitochondrial NAD^+:NADH ratio (Bilan et al., 2014). SoNar, a highly sensitive cpYFP and Rex-based reporter of NADH and NAD^+ levels, has yet to be targeted to mitochondria (Zhao et al., 2015). The use of cpYFP, however, is limited by its pH sensitivity, and any cpYFP reporters need to be used in conjunction with a pH reporter.

Peredox, consisting of two FPs (T-Sapphire and mCherry) and a Rex dimer, reports the free cytosolic NADH:NAD^+ ratio with a high affinity for NADH (Hung et al., 2011). Peredox is mostly pH insensitive, but thus far has not been successfully utilised to measure mitochondrial NADH:NAD^+, likely due to its sub-optimal sensitivity range (NADH:NAD^+ ratios are estimated to be >20 fold

higher in the mitochondria than in the cytoplasm (Hung et al., 2011)). Genetically-encoded reporters of mitochondrial NAD^+ and NADPH have also been developed recently (Cambronne et al., 2016, Tao et al., 2017). Because of the predominance of NAD^+ over NADH, small changes in NAD^+ could be missed using ratio reporters, making NAD^+ sensors a promising development, especially considering the recent interest in ageing and NAD^+-dependent sirtuin activity (Fang et al., 2016, Cambronne et al., 2016).

5.5. Respiratory complex activity and subunit expression

Reduced expression or activity of respiratory complexes has been reported in most NDs, as described earlier. These changes, however, may not necessarily translate into compromised mitochondrial function, due to variations in rate-limiting factors, the distribution of control along the respiratory chain or the presence of compensatory mechanisms (e.g. between Complex I and II) (Brand and Nicholls, 2011). For this reason, assays measuring subunit expression or complex activity may be more usefully employed to investigate the specific molecular origin of a known mitochondrial defect, rather than as a general measure of mitochondrial bioenergetic function. Such investigations may be complemented by OCR measurements in permeabilised cells or isolated mitochondria, where the provision of different substrates can isolate specific complex activity.

5.5.1. Experimental Protocol

Protein levels of specific subunits of the respiratory complexes (Complexes I-IV and the F_1F_o ATP synthase) can be assessed by Western Blotting with individual antibodies or commercially available antibody cocktails (e.g. MitoProfile® from Mitosciences, Abcam). As some antibodies bind to auxiliary rather than catalytic subunits, altered subunit expression in these instances may not correspond to altered complex activity.

The activity of the respiratory complexes can be measured via histochemical staining of fresh frozen brain tissue (e.g. cytochrome *c* oxidase (COX) and/or succinate dehydrogenase (SDH) staining; (Ross, 2011), with in-gel enzymatic histochemical reactions (Jung et al., 2000), or with spectrophotometric assays (commercially available kits, or see below). Complex activity can be measured in tissues, cells, mitochondria-enriched fractions or isolated mitochondria. Activity has also been measured in pre-synaptic nerve terminals (synaptosomes) (Sipos et al., 2003), but these preparations can be hampered by heterogeneity (Nicholls, 2006). Although isolating mitochondria from cellular homogenates is a delicate and time-consuming procedure and experimental data can vary based on the quality of the isolation, it is nevertheless required for many assays to reduce the confounding contribution of non-mitochondrial enzymes (Spinazzi et al., 2012) and to increase assay sensitivity. Measurement of respiratory complex activity also requires appropriate disruption of the mitochondrial membrane. Spectrophotometric assays involve mixing the mitochondrial content with electron donors and acceptors appropriate for the complex being studied, and measuring the change in absorbance at the appropriate wavelength for the specific electron donor/acceptor (Table 3). The activity of the ANT can also be measured in permeabilised cells (Chinopoulos et al., 2014).

Table 3: Description of spectrophotometric enzymatic assays to measure respiratory complex activity. Protocols for a variety of assays can be found on manufacturers' websites for commercially available assays (e.g. the MitoTox™ suite from MitoSciences, or MitoCheck® from Cayman), and in various publications (e.g. (Sipos et al., 2003, Barrientos et al., 2009, Spinazzi et al., 2012)). Respiratory chain complex activities can be normalised to the amount of protein in the sample, or to citrate synthase activity (Barrientos et al., 2009, Spinazzi et al., 2012).

Respiratory complex (synonyms)	**Enzymatic assay description**
Complex I (NADH:ubiquinone oxidoreductase, NADH dehydrogenase, EC 1.6.5.3)	In catalysing the oxidation of NADH to NAD^+, Complex I transfers electrons from NADH to ubiquinone (coenzyme Q_{10}). Assays to measure Complex I activity therefore utilise NADH as the electron donor, and a ubiquinone analog (e.g. coenzyme Q_1 or decylubiquinone, DB) as the electron acceptor. Activity is determined by measuring the rate of oxidation of NADH to NAD^+, or less frequently by measuring the rate of reduction of the ubiquinone analog. The rate of NADH oxidation is measured by tracking the decrease in absorbance of the sample at 340 nm, or DB reduction can be followed at 247-272 nm. The majority of Complex I activity should be rotenone-sensitive.
Complex II (succinate-ubiquinone oxidoreductase, succinate dehydrogenase)	Complex II oxidises succinate to fumarate, while reducing ubiquinone to ubiquinol. In this assay, succinate is used as the electron donor with dichlorophenolindophenol (DCPIP) the electron acceptor. Complex II activity can be measured by following the decrease in absorbance at 600 nm caused by the reduction of DCPIP. Complex II activity should be sensitive to malonate. Rotenone and antimycin A are usually added to minimise the endogenous ubiquinone accepting electrons from Complex II (and the resultant underestimation of Complex II activity).
Complex III (ubiquinol-cytochrome *c* oxidoreductase, EC 1.10.2.2)	In catalysing the reduction of cytochrome *c*, complex III transfers electrons from ubiquinol to cytochrome *c*. A ubiquinone analog (such as DB) is therefore used as the electron donor, while cytochrome *c* is used as the electron acceptor. Complex III activity is measured by following the increase in absorbance at 550 nm caused by the reduction of cytochrome *c*. The rate of oxidation of the ubiquinone analog can also be monitored. The majority of Complex III activity should be sensitive to antimycin A. Cyanide (CN) or another Complex IV inhibitor should be added to prevent cytochrome *c* oxidation.
Combined complex I	The rate of reduction of cytochrome *c* (electron acceptor), using NADH

and complex III (NADH-cytochrome *c* oxidoreductase)	as the electron donor (Complex I substrate), is measured by monitoring the increase in absorbance at 550 nm. CN or another Complex IV inhibitor should be added to prevent cytochrome *c* oxidation.
Combined complex II and III (succinate-cytochrome *c* oxidoreductase)	The rate of reduction of cytochrome *c* (electron acceptor), using succinate as the electron donor (Complex II substrate), is measured by tracking the increase in absorbance at 550 nm. CN or another Complex IV inhibitor should be added to prevent cytochrome *c* oxidation.
Complex IV (cytochrome *c* oxidase, EC 1.9.3.1)	Complex IV transfers electrons from cytochrome *c* to molecular oxygen, converting oxygen to water. To measure Complex IV activity, reduced cytochrome *c* (ferrocytochrome *c*) is used as the electron donor. Complex IV activity is measured by the decrease in absorbance at 550 nm, caused by oxidation of cytochrome *c*. The majority of complex IV activity is sensitive to potassium cyanide (KCN).
F_1F_o ATP synthase	The activity of the F_1F_o ATP synthase (assayed as the reverse ATPase activity) is more difficult to measure, due to a high level of oligomycin-resistant ATPase activity (Spinazzi et al., 2012). Assays can be performed that infer the reverse activity of ATP synthase (ATP hydrolysis to ADP) by measuring the lactate dehydrogenase-driven oxidation of NADH to NAD^+. These reactions are coupled by the activity of pyruvate kinase which supplies pyruvate to fuel lactate dehydrogenase while generating ATP to fuel the ATP synthase reverse activity. Enzyme activity is measured by tracking the decrease in absorbance at 340 nm caused by NADH oxidation (Barrientos et al., 2009).

5.5.2. Experimental analysis

Enzymatic activity ($nmol.min^{-1}.mg^{-1}$) is calculated using the Beer-Lambert law

$$Enzymatic\ activity\ = \frac{\Delta Absorbance.min^{-1}\ x\ 1000}{e_\lambda\ x\ V\ x\ Protein\ conc.}$$

where e_λ = extinction coefficient ($mM^{-1}.cm^{-1}$)
= ~6.2 for NADH @ 340 nm, ~20 for DCPIP @ 600 nm, ~19 for reduced cytochrome *c* – oxidised cytochrome *c* @ 550 nm (difference extinction coefficient) (Spinazzi et al., 2012, Barrientos et al., 2009)

V = volume of sample (ml)

Protein conc. = protein concentration of sample ($mg.ml^{-1}$)

5.6. Fluorescent reporters of mitochondrial ATP, calcium (Ca^{2+}) and pH

Mitochondrial ATP, Ca^{2+} and pH, as well as other metabolites and ions, can be monitored using fluorescent dyes or genetically-encoded fluorescent reporters. Genetically-encoded fluorescent reporters generally comprise one or two fluorescent proteins (FPs) connected to a peptide/protein whose conformation is altered by the target molecule or event (Tantama et al., 2012, San Martin et al., 2014). For example, the conformation of the peptide/protein may be altered when bound by a certain ligand (e.g. ATP or glucose), or cleaved or phosphorylated by an enzyme (e.g. caspases or AMPK). This conformational change alters the fluorescent properties of the reporter, providing a detectable measure of the concentration of the ligand, or the activity of the enzyme. Caveats for all genetically-encoded fluorescent reporters include; sensitivity to environmental factors such as pH (can be corrected for with simultaneous use of a pH sensor), buffering of the target molecule (especially relevant for low abundance molecules), non-specificity (availability of negative controls is important), and the functional impact of the introduction of an exogenous, sometimes large, protein (Tantama et al., 2012).

Förster resonance energy transfer (FRET)-based fluorescence reporters commonly comprise two FPs connected by a linker peptide/protein, with the emission spectra of one FP (donor) overlapping the excitation spectra of the other (acceptor). With both FPs in close physical proximity (< ~10 nm), FRET occurs from the donor to the acceptor (energy transferred from the donor excites the acceptor), reducing the donor, and increasing the acceptor, fluorescence intensity (Figure 5). Since FRET is proportional to the 6^{th} power of the distance between the FPs, any conformational change in the linker protein that minimally alters the distance between and/or the orientation of the FPs, can induce considerable FRET changes. The occurrence of FRET actually affects several fluorescence parameters, such as the emission intensity of the FPs at constant excitation, and their fluorescence decay time. The former has been used most frequently because of its relative simplicity to measure, limited cost, and high velocity of image acquisition. Fluorescence decay or lifetime imaging microscopy (FLIM) instead requires a dedicated apparatus, but it offers the advantage of being relatively insensitive to some experimental conditions such as focus drift, bleaching, or excitation light fluctuation. This technique is utilised in Enhanced Acceptor Fluorescence (EAF), where both fluorophores are excited at the same wavelength (~480 nm for GFP-YFP pairs) and the average lifetime of the emitted fluorescence is measured (Harpur et al., 2001). As YFP has a longer lifetime than GFP, the average lifetime will increase when the two FPs are in close enough proximity for FRET to occur (more YFP contributing to the average lifetime). Ratiometric measurements (such as provided by FRET-based reporters) facilitate intra-experimental normalisation and reduce the effects of volume changes, focus drift and reporter concentration. Fluorescent reporters can be multiplexed to allow simultaneous monitoring of multiple processes (e.g. cyan FP (CFP)/YFP FRET-based reporters in conjunction with red fluorescent reporters, such as TMRM (Connolly et al., 2014)).

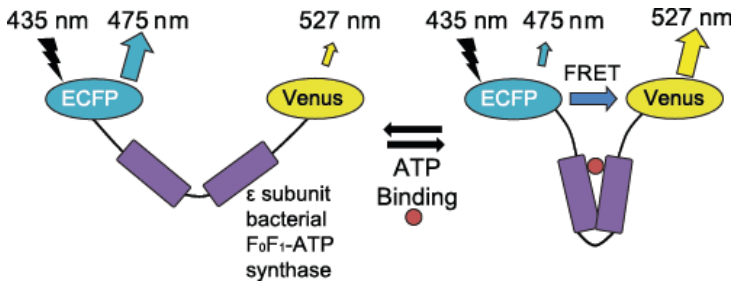

Figure 5: Schematic of ATeam, a FRET-based reporter of ATP (Imamura 2009). The reporter comprises a linker protein (ε-subunit of a bacterial F_1F_o ATP synthase) inserted between a donor CFP and acceptor YFP (enhanced CFP and Venus). ATP binding induces a conformational change in the linker protein, increasing FRET between the two FPs and altering the emitted fluorescence. Ratiometric measurements are obtained by calculating the FRET ratio (CFP/YFP). The acceptor YFP can also be laser-excited at ~488 nm. Fluorescent emissions from both FPs should be monitored, to ensure that any ratio change is due to altered FRET (opposite changes in the fluorescence of the individual FPs), rather than other sources (such as increased auto-fluorescence). Image reproduced with permission from (Connolly et al., 2014).

Genetically-encoded fluorescent reporters can be transfected into primary neurons using a variety of techniques, such as lipofection, Ca^{2+} phosphate co-precipitation or Amaxa nucleofection (Lonza) (Karra and Dahm, 2010). Many of these techniques, however, are hampered by high toxicity and low transfection efficiency in primary cells. Lenti- or adeno-viral approaches can improve transduction efficiency (Karra and Dahm, 2010). Fluorescent reporters can be modified to target the reporter to the mitochondrial membrane, matrix or inter-membrane space. Targeting fluorescent reporters to mitochondria, however, is not without challenges – the size or complexity of the reporter may limit its ability to translocate into mitochondria, the increased basicity of mitochondria (~pH 8) may impact reporter function, and mitochondrial metabolites may affect reporter readout (Tantama et al., 2012, De Michele et al., 2014). Mitochondrial localisation of transfected reporters (and fluorescent dyes) should be verified, by e.g. co-localisation with an established mitochondrial marker. It is also good practice to confirm that the mitochondrial targeting of the fluorescent reporter does not disrupt mitochondrial respiratory function, by e.g. measuring OCR according to Protocol 1.

Accurate calibration of a fluorescent reporter can sometimes provide absolute quantification of metabolite, ion or protein concentrations. Nevertheless, changes in steady-state concentration can be due to any number of processes, including altered import, export, synthesis or consumption - experiments are required to further delineate the contributing factors.

5.6.1. Mitochondrial ATP

The ATeam FRET-based reporters of ATP concentration (Imamura et al., 2009) comprise the ATP-binding ε subunit of the bacterial F_1F_o ATP synthase from *Bacillus subtilis* inserted between CFP and YFP variants (msECFP and cpVenus). Specific and reversible binding of ATP to the ε subunit induces a conformational change in the ATeam reporter, increasing the FRET-induced fluorescence intensity. The ATeam AT1.03 subtype, with a dissociation constant (K_d) of 3.3 mM for ATP at 37 °C, can detect ATP fluctuations in the mM range (less sensitive to smaller changes), and can be used with the mutated AT1.03R122K/R126K negative control (Imamura et al., 2009). This affinity is highly temperature dependent, varying five-fold over a range of 10 °C (Imamura et al., 2009). AT1.03 fluorescence is stable over physiological pH (7.1-8.5; mitochondrial pH ~8.0), but changes outside this range may affect fluorescence. ATeam variants have been localised to mitochondria (mitoATeam) and successfully utilised in neurons (Imamura et al., 2009, Barsukova et al., 2011). The red-shifted mitoGO-ATeam, comprising GFP and orange FP variants (cp173-mEGFP and mKO_k), is less phototoxic, less sensitive to pH and enables multiplexing with UV excitable probes, such as the fluorescent Ca^{2+} indicator Fura-2 (the excitation spectra of CFP, used in the ATeam reporter, is in the UV range) (Nakano et al., 2011, Rueda et al., 2015).

The ATP/ADP ratio is a more complete measure of cellular energy status than ATP alone (Tantama et al., 2013). The PercevalHR reporter is a dual-excitation fluorescent reporter of the ATP/ADP ratio that can reliably detect ratios from ~0.4-40 (Berg et al., 2009, Tantama et al., 2013), with ATP/ADP ~10 in cultured neurons at rest (Katsura et al., 1993). However, PercevalHR is sensitive to pH changes within the physiological range (6.7-7.8), requiring simultaneous pH monitoring, and to our knowledge has not yet been successfully utilised in mitochondria. pH sensitivity is especially problematic in neurons, where intracellular acidification often occurs with decreases in ATP, such as during excitotoxicity. Other fluorescence-based ATP sensors, such as the dual-excitation, single FP ATeam variant, QUEEN-2m (Yaginuma et al., 2014), and a potential EAF-based ATP biosensor (developed in (Zadran et al., 2013), although lifetime measurements were not performed), have yet to be targeted to mammalian mitochondria.

A bioluminescence energy transfer (BRET) probe (BTeam) has recently been developed (Yoshida et al., 2016). Bioluminescence-based probes avoid the excitation light required for fluorescence-based imaging, but emitted bioluminescence is generally weaker than fluorescent signals (necessitating lengthy exposure) and the technique requires the addition of a luciferase substrate (furimazine in the case of BTeam,). BTeam comprises the same ATP-binding ε subunit as the ATeam probe, inserted between a non-ATP-consuming NanoLuciferase (NLuc; emission peak ~455 nm), and a YFP variant (mVenus). Changes in the BRET ratio (YFP/Nluc) can report ATP fluctuations between 0-10 mM, and the probe can be targeted to mitochondria (mit-BTeam). Similar to the ATeam probe, BTeam

measurements are stable within physiological pH (7.1-8.3) but are sensitive to temperature changes (Yoshida et al., 2016).

Mitochondrial ATP can also be measured in isolated mitochondria using a number of single time-point techniques, such as luciferase bioluminescence assays (which also exhibit pH sensitivity), high performance liquid chromatography (HPLC), or ^{31}P NMR (Rajendran et al., 2016).

Table 4: Genetically-encoded fluorescent reporters of ATP that have been successfully targeted to neuronal mitochondria. Publications refer to the work that originally generated the probe and studies where the probe was utilised in neuronal mitochondria.

Reporter name	**Reporter detail**	**Excitation/emission wavelengths (nm)**	**Dissociation constant (K_d)**	**References**
mitoATeam (mitAT1.03)	CFP-YFP FRET	CFP (mECFP): 435/475 YFP (cpVenus): 515/527	3.3 mM	(Imamura et al., 2009, Barsukova et al., 2011)
Mit GO-ATeam 2	GFP-OFP FRET	GFP (mEGFP): 470/510 OFP (mKO_k): 550/560	2.3 mM	(Nakano et al., 2011, Rueda et al., 2015)

5.6.2. Mitochondrial Ca^{2+}

Mitochondria play a major role in Ca^{2+} signalling and homeostasis through its uptake, sequestration, and release (De Stefani et al., 2016). Thanks to the large electrochemical gradient across its inner membrane (proton-motive force), mitochondria can import huge amounts of Ca^{2+} through the mitochondrial Ca^{2+} uniporter (MCU) complex, and serve as buffers in periods of high cytoplasmic Ca^{2+} such as during neuronal excitation or excitotoxicity (Nicholls and Budd, 2000, Qiu et al., 2013). Within mitochondria, Ca^{2+} regulates substrate import, several TCA cycle dehydrogenases, components of the respiratory chain and ATP synthesis, coupling neuronal excitation/activity with bioenergetics (Kann and Kovacs, 2007, Llorente-Folch et al., 2015). Ca^{2+} is released from neuronal mitochondria primarily through the Na^{+}/Ca^{2+} exchanger NCLX (Kann and Kovacs, 2007, Palty et al., 2010, De Stefani et al., 2016). Excessive mitochondrial Ca^{2+}, however, can be toxic, contributing to increased ROS production, activation of the mitochondrial permeability transition pore, delayed Ca^{2+} deregulation and neuronal death (Pivovarova and Andrews, 2010). Such mitochondrial Ca^{2+} overload and subsequent dysfunction have been implicated in neurodegeneration (Bezprozvanny and Mattson, 2008).

In the following discussion, it must be borne in mind that fluorescent indicators monitor free, rather than total, Ca^{2+}. Under conditions of high matrix loading, for example when modelling excitotoxicity, formation of a Ca^{2+}-phosphate complex can mean that, although total matrix Ca^{2+} can approach 1 M, free Ca^{2+} is in the low μM range. Electron probe microanalysis or $^{45}Ca^{2+}$ studies are needed to monitor total Ca^{2+} concentration. It is also important to remember that these reporters act as Ca^{2+} buffers, and may alter the endogenous ion dynamics (Grienberger and Konnerth, 2012).

Several fluorescent reporters are available to measure free mitochondrial Ca^{2+} (Table 5). The positively charged fluorescent Ca^{2+} indicator Rhod-2 (and its analogs) are imported by mitochondria, but accumulate only incompletely and can alter intracellular Ca^{2+} dynamics (Kann and Kovacs, 2007, Pozzan and Rudolf, 2009, Rysted et al., 2017). Although such reporters do not require transfection, they have generally been superseded by genetically-encoded Ca^{2+} indicators that can be targeted to mitochondria.

Cameleons are FRET-based Ca^{2+} sensors comprising two FPs (the more recent 'yellow cameleons' (YC) utilise eCFP and cpVenus (Nagai et al., 2004)) connected by a Ca^{2+}-binding protein, calmodulin (CaM), and a CaM-binding peptide of myosin light-chain kinase, M13. CaM-Ca^{2+} binding leads to a CaM-M13 interaction that induces a conformational change in the reporter, altering the FRET efficiency and emitted fluorescence (Miyawaki et al., 1999). Cameleons have been optimised for brightness and increased dynamic range (YC3.60; (Nagai et al., 2004)), and to reduce off-target interactions (D3cpv; (Palmer et al., 2006)). Replacing CaM with troponin C can also reduce off-target binding in neurons (Grienberger and Konnerth, 2012). The mitochondria-targeted 4mtD2cpv –

4mtD4cpv series of Cameleons with varying Ca^{2+} affinities (Palmer et al., 2006) have been successfully used in primary neurons (Qiu et al., 2013).

Smaller, single protein-based Ca^{2+} indicators may localise more easily to mitochondria (De Michele et al., 2014). Aequorin, a jellyfish protein that bioluminesces in a Ca^{2+}-dependent manner, can be localised to neuronal mitochondria (mtAEQ) (Rizzuto et al., 1992, Bonora et al., 2013), but its low luminescence intensity limits its utility in single-cell measurements (Pozzan and Rudolf, 2009). Other single FP-based Ca^{2+} indicators that have been successfully imaged in neuronal mitochondria (Table 5) include the cpYFP-based Pericam (Nagai et al., 2001) and multiple variants of GCaMP and RCaMP (Nakai et al., 2001, Chen et al., 2011, Qiu et al., 2013, Akerboom et al., 2013). GECO Ca^{2+} reporters (Zhao et al., 2011a), variants of GCaMP3, have been used extensively to measure mitochondrial Ca^{2+} in neurons (Llorente-Folch et al., 2013, Wu et al., 2014, Rueda et al., 2015, Rysted et al., 2017). CEPIA probes are GCaMP2 variants that can be localised to mitochondria (Suzuki et al., 2014). Luminescence-based methods (BRET) are also promising (Suzuki et al., 2016). Mitochondria-targeted reporters can be co-expressed with fluorescent Ca^{2+} indicators designed for other subcellular locations (e.g. endoplasmic reticulum or cytoplasm) to simultaneously monitor Ca^{2+} flux between cellular compartments (Wu et al., 2014, Rysted et al., 2017).

These and other Ca^{2+} reporters are extensively reviewed elsewhere e.g. (Pendin et al., 2015, Rysted et al., 2017). The final choice of reporter depends on the probe's affinity, dynamic range and available equipment. Reporters should be calibrated to identify their dynamic range in the specific experimental setting – this involves determining F_{max}/F_{min} or R_{max}/R_{min} for non-ratiometric and ratiometric dyes, respectively, where F_{max} (R_{max}) is the fluorescence intensity (ratio) at saturating Ca^{2+} concentrations, and F_{min} (R_{min}) is the fluorescence intensity (ratio) at minimal/zero Ca^{2+} concentrations (Palmer et al., 2006, Rudolf et al., 2003). Ionomycin, typically used for F_{max}/F_{min} determination, will take longer to saturate reporters localised within mitochondria. These values can be used, along with the reporter's dissociation constant (K_d), to calculate relative Ca^{2+} concentrations (Rudolf et al., 2003, Rysted et al., 2017).

Table 5: Several genetically-encoded fluorescent and bioluminescent reporters of Ca^{2+} with varying affinities (K_d) that have been successfully targeted to neuronal mitochondria. Publications refer to the work that originally generated the probe and/or studies where the probe was utilised in neuronal mitochondria. Multiple mitochondria-localised Ca^{2+} reporters based on GCaMP have been generated.

Reporter name	Reporter detail	Excitation, emission wavelengths (nm)	Dissociation constant, K_d (μM)	References
Rhod-2	Fluorescent molecule	λ_{ex} ~557 λ_{em} ~581	0.6*	(Qiu et al., 2013)
4mtD2cpv **4mtD3cpv** **4mtD4cpv**	Yellow cameleon (FRET)	CFP (ECFP): $\lambda_{ex}/\lambda_{em}$ 435/475 YFP (cp173Venus): $\lambda_{ex}/\lambda_{em}$ 515/527	4mtD2cpv: 0.1, 7.7 4mtD3cpv: 0.76 4mtD4cpv: 49.7	(Palmer et al., 2006, Qiu et al., 2013)
mtAEQmut	Aequorin (bioluminescence)	λ_{em} 465	Varying affinities (Bonora et al., 2013)	(Rizzuto et al., 1992, Bonora et al., 2013)
Mit-GEM-GECO-1	Single FP, dual emission, ratiometric	λ_{ex} 390 λ_{em} 455, 511	0.34	(Zhao et al., 2011a, Llorente-Folch et al., 2013, Rueda et al., 2015)
Mito-LAR-GECO1.2	Single FP (RFP)	λ_{ex} 557 λ_{em} 584	12	(Wu et al., 2014)
mito-GCaMP2	Single FP (cpEGFP)	λ_{ex} 489 λ_{em} 509	0.2	(Nakai et al., 2001, Chen et al., 2011, Qiu et al., 2013)
mt-RCaMP	Single FP (cp-mRuby)	λ_{ex} 570 λ_{em} 590	1.6	(Akerboom et al., 2013)
mtPericam	Dual-excitation, ratiometric	λ_{ex} 415, 494 λ_{em} 515	1.7	(Nagai et al., 2001, Barsukova et al., 2011)

* Rhod-2 analogs have varying affinities.

5.6.3. Mitochondrial pH (pH_{mito})

Knowledge of the mitochondrial matrix pH and ΔpH_m ($pH_{mito} - pH_{cyto}$), in conjunction with $\Delta\psi_m$, allows calculation of the proton-motive force (Δp), with ΔpH_m contributing ~20-30 % of Δp (Perry et al., 2011). ΔpH_m regulates the flux of several metabolites across the mitochondrial membrane (Santo-Domingo and Demaurex, 2012), and changes in pH_{mito} often occur with energy metabolism fluctuations. pH_{mito} measurements can also be used to correct for experiments involving genetically-encoded FPs or other reporters exhibiting pH-sensitivity. Conversely, many pH-sensitive FPs have themselves been adapted for use as direct pH sensors (Bencina, 2013). For pH_{mito} measurements, reporters with a high acid dissociation constant (pK_a >7.5) are required, appropriate for the higher pH of mitochondria (more alkaline) compared to the cytosol (Santo-Domingo and Demaurex, 2012, Bencina, 2013).

Although pH-sensitive fluorescent dyes exist (e.g. SNARF, BCECF), they are not specifically targeted to mitochondria, necessitating the concomitant use of a fluorescent mitochondrial marker (Santo-Domingo and Demaurex, 2012). pH_{mito} is more commonly measured using genetically-encoded FPs. YFP variants can be used to measure pH_{mito}, as YFP is more pH-sensitive than GFP. Single FP reporters using EYFP, for example, have been targeted to the mitochondrial intermembrane space (MIMS-EYFP) and matrix (mt-YFP, mitoYFP) in neurons (Porcelli et al., 2005, Bolshakov et al., 2008, Barsukova et al., 2011). The pH indicator pHluorin (Miesenbock et al., 1998) has also been targeted to mitochondria (Vijayvergiya et al., 2004). The pK_a of EYFP and pHluorin (~7 and 7.1, respectively), however, are not optimal for measurement of pH_{mito} (Bencina, 2013).

SypHer, a dual-excitation ratiometric probe (pK_a 8.7; excitation 430, 490 nm; emission ~535 nm (Poburko et al., 2011)), harnesses the inherent pH sensitivity of cpYFP, and was generated from the hydrogen peroxide sensor HyPer. The mitochondria-targeted variant, mitoSypHer, has been used to measure neuronal pH_{mito} (Breckwoldt et al., 2016). mtAlpHi (mitochondrial alkaline pH indicator, pK_a ~8.5), is a non-ratiometric, intensity-based pH indicator that has also been targeted to neuronal mitochondria (Abad et al., 2004). mtAlpHi was generated from the Ca^{2+} indicator Camgaroo2, with CaM replaced by a Ca^{2+}-insensitive aequorin segment. Other pH-sensitive fluorescent indicators suitable for reporting pH_{mito} include pHRed (pK_a 7.8), which can also be used for FLIM (Tantama et al., 2011), and pHTomato (pK_a 7.8; (Li and Tsien, 2012)).

Table 6: Genetically-encoded fluorescent reporters of pH that have been successfully targeted to neuronal mitochondria. Publications refer to the work that originally generated the probe and studies where the probe was utilised in neuronal mitochondria. See text for more details.

Reporter name	Reporter type	Excitation, emission wavelength (nm)	pK_a	References
MIMS-EYFP	Single FP (EYFP)	λ_{ex} ~513 λ_{em} ~530	~7.0	(Porcelli et al., 2005, Bolshakov et al., 2008)
mt-EYFP, mito-EYFP	Single FP (EYFP)	λ_{ex} ~513 λ_{em} ~530	~7.0	(Porcelli et al., 2005, Barsukova et al., 2011)
mitoSypHer	Single FP (cpYFP), dual-excitation, ratiometric	λ_{ex} ~430, ~490 λ_{em} ~535	~8.7	(Poburko et al., 2011, Breckwoldt et al., 2016)
mtAlpHi	Single FP (EYFP) chimera	λ_{ex} ~500 λ_{em} ~520	~8.5	(Abad et al., 2004)

5.7. Mitochondrial reactive oxygen species

Reactive oxygen species (ROS) are a group of reactive molecules derived from oxygen, and include superoxide (O_2^-), hydrogen peroxide (H_2O_2) and hydroxyl radicals ($^{\bullet}OH$). Mitochondria, as the primary oxygen consumers within the cell, play a critical role in ROS metabolism, as electrons leaked from components of the OxPhos machinery can react with O_2 to form superoxide (O_2^-) (Dickinson et al., 2010, Murphy, 2009). Mitochondria-derived O_2^- is rapidly converted (dismutated) to H_2O_2 by superoxide dismutase (SOD2/MnSOD in the mitochondrial matrix; SOD1 in the inter-membrane space and cytoplasm), but can also be converted to the toxic reactive nitrogen species, peroxynitrite, by reaction with nitric oxide (Murphy, 2009, Polster et al., 2014). H_2O_2 can in turn create more reactive oxygen by-products such as $^{\bullet}OH$ (Polster et al., 2014). Together, ROS are vital second messengers and play a key role in redox-dependent signalling, but ROS accumulation, such as following hypoxia-ischaemia-reperfusion injury or excitotoxicity, contributes to oxidative stress and has been associated with ageing and neurodegeneration (Yin et al., 2014, Lin and Beal, 2006). The precise effects of specific ROS and their associated anti-oxidants vary considerably throughout the cell (Murphy et al., 2011).

The primary sources of mitochondrial O_2^- are Complexes I and III, and TCA cycle enzymes (Sipos et al., 2003, Kann and Kovacs, 2007, Murphy, 2009), while the assembly of Complex I into supercomplexes can dictate the rate of ROS formation (Lopez-Fabuel et al., 2016). Increased respiration and a hyperpolarised mitochondrial membrane can increase ROS production in neurons (Nicholls and Budd, 2000, Bindokas et al., 1996, Garcia et al., 2005). Conversely, inhibition of the respiratory complexes can also increase ROS production (Sipos et al., 2003), when the mitochondrial membrane potential may be maintained by reverse activity of the F_1F_o ATP synthase and ROS are generated through electron leaks (Abramov et al., 2007, Brennan et al., 2009). ROS generation is therefore strongly regulated by respiration, with the underlying factors disrupting respiration likely determining the ROS response (Adam-Vizi and Chinopoulos, 2006, Brand, 2016).

5.7.1. Experimental set-up

ROS levels can be inferred by imaging redox-sensitive fluorophores or genetically-encoded FPs, by measuring the activity of redox-sensitive enzymes such as aconitase, or by detecting probe oxidation products using methods such as electron paramagnetic resonance spectroscopy or HPLC (Nicholls and Budd, 2000, Dickinson et al., 2010, Polster et al., 2014, Woolley et al., 2013). Recent developments in ROS-sensitive measurements involve the use of inert nanoparticles or carbon nanotubes (Uusitalo and Hempel, 2012, Woolley et al., 2013), although these approaches have yet to be tested in neuronal mitochondria.

We strongly stress that current methods for measuring mitochondrial ROS, particularly redox-sensitive fluorophores, are associated with significant difficulties and limitations that must be carefully considered, both when interpreting the existing literature and during experiment design. These difficulties are associated with, among others, signal specificity, identifying the intracellular origin of ROS, and the rapid turnover of ROS within the cell. If performing experiments, stringent control measures must be employed, all findings should be interpreted with caution, and results should be confirmed using alternative techniques e.g. (Vincent et al., 2005). Many of these issues have been discussed previously (Chen et al., 2010, Zielonka and Kalyanaraman, 2010, Murphy et al., 2011, Polster et al., 2014), and technical specifications, use guidelines and limitations of several redox-sensitive fluorophores and FPs can be found in (Woolley et al., 2013, Booth et al., 2016, Can et al., 2017).

Redox-sensitive fluorophores

Redox sensitive fluorophores can be tracked with live cell microscopy or detected using fixed time-point techniques such as flow-cytometry or microplate readers. These molecules are frequently targeted to mitochondria by using lipophilic cations, taking advantage of the negative potential across the mitochondrial inner membrane (Dickinson et al., 2010). This means, however, that any readout cannot be reliably attributed to mitochondrial ROS generation in conditions of mitochondrial depolarisation (as is commonly the case in studies of neurodegeneration) without some form of correction (Polster et al., 2014, Abramov et al., 2007, Brennan et al., 2009). As with all fluorescent dyes, and especially for those expected to localise to mitochondria, cells should be allowed to equilibrate the dye for at least 30 min prior to imaging. Removal of charge-sensitive fluorophores from the media may lead to re-equilibration across membranes and dilution of signal intensity. As the fluorescence of ROS-sensitive fluorophores increases over an experiment (due to accumulation of irreversibly oxidised dye), the initial measured fluorescence is dependent on loading time (Hempel et al., 1999), and laser settings (intensity, gain) should be adjusted for low fluorescence to avoid subsequent saturation. The slope of the increase in fluorescence is calculated as a measure of the steady-state ROS level over the time measured (Abramov et al., 2007, Nicholls and Budd, 2000). We here introduce, and discuss the issues associated with, the most commonly utilised redox-sensitive fluorescent probes – an extensive description of other probes is provided in (Woolley et al., 2013).

The blue-fluorescent dihydroethidium (hydroethidine; HEt) is oxidised by O_2^- to the red fluorescent 2-hydroxyethidium, but can also be oxidised by other ROS to the red fluorescent ethidium and other non-fluorescent by-products (Zielonka and Kalyanaraman, 2010, Polster et al., 2014). Conjugating HEt to the positively charged, lipophilic triphenylphosphonium cation (TPP^+) allows HEt to localise to mitochondria (mito-HEt/MitoSOX Red (Invitrogen/ThermoFisher)). MitoSOX is excited at 543 nm

and its emission detected at ~585 nm (although ~408 nm excitation may be somewhat more specific for 2-hydroxyethidium (Robinson et al., 2008)). Unfortunately, a number of issues exist to confound HEt-based mitochondrial ROS measurements. As the fluorescent spectra of 2-hydroxyethidium and ethidium overlap, HEt cannot distinguish between different types of ROS without the aid of additional techniques such as HPLC (Robinson et al., 2008, Zielonka and Kalyanaraman, 2010). Once oxidised, HEt binds to DNA and RNA, which increases its fluorescence. Positively charged HEt oxidation products can accumulate in the negatively charged mitochondria (dependent on $\Delta\psi_m$), regardless of their source (Zielonka and Kalyanaraman, 2010). Following mitochondrial depolarisation, these products can also redistribute to the nucleus, significantly increasing fluorescence due to DNA binding and nucleic acid intercalation (Polster et al., 2014). Together, this means that the localisation of the fluorescent signal does not inform about where the oxidation took place, even if the nucleus is not imaged. MitoSOX is oxidised by photo-toxicity, so low concentrations (0.1-0.2 μM in several types of cultured neurons) and minimal laser intensities are required (Polster et al., 2014). Low concentrations also reduce the binding capacity of HEt to mitochondrial DNA, and the MitoSOX-induced impairment of mitochondrial metabolism (Polster et al., 2014, Roelofs et al., 2015). Finally, some drugs interact with HEt-derived compounds, such as high concentrations of the Complex III inhibitor, antimycin A, or the ROS scavenger MnTBAP (Polster et al., 2014, Zielonka and Kalyanaraman, 2010). Guidelines on the utility, optimisation and imaging of MitoSOX in neurons have been provided recently (Polster et al., 2014).

Dihydrorhodamine 123 (excitation/emission 500/536 nm), whose emission spectra is also altered by irreversible non-specific oxidation, localises to mitochondria due to its positive charge (Dugan et al., 1995) and is therefore strongly $\Delta\psi_m$-dependent. Indeed, its oxidised product, rhodamine 123, is itself used as an indicator of $\Delta\psi_m$. Derivatives of dichlorofluorescein (DCF) (excitation/emission 488/510 nm) only penetrate the outer mitochondrial membrane, and are associated with other issues, including a non-linear fluorescence response (Hempel et al., 1999, Chen et al., 2010). MitoPY1 (Mitochondrial peroxy yellow), a hybrid fluorescein/rhodamine reporter, may selectively report mitochondria-derived H_2O_2 (Dickinson et al., 2013). Similar to HEt-based fluorophores, however, these reporters are associated with significant limitations, such as lack of specificity, auto- and photo-oxidation, and pH sensitivity (Hempel et al., 1999, Nicholls and Budd, 2000, Chen et al., 2010, Murphy et al., 2011, Can et al., 2017).

As H_2O_2 is fully membrane-permeable, release of H_2O_2 is sometimes used to infer mitochondrial ROS production, especially in isolated mitochondria – Amplex Red (Molecular probes) is a sensitive and stable probe that reacts with H_2O_2 (in the presence of HRP) to produce the highly fluorescent resorufin, which can be detected by colorimetric or fluorimetric readers (excitation/emission at 570/585 nm) (Sipos et al., 2003). However, some mitochondrial H_2O_2 will be consumed prior to its

release from mitochondria, and the contribution to the signal from non-mitochondrial sources of ROS is significant and cannot be discounted if performing measurements in intact cells (Murphy, 2009).

Redox-sensitive fluorescent proteins

Due to the myriad issues with redox-sensitive fluorophores, the use of mitochondria-targeted redox-sensitive FPs may be more appropriate, although they are prone to similar issues associated with the uncertainty over the origin of ROS, and its rapid turnover. In contrast to fluorophores, redox-sensitive FPs reversibly react with ROS and can therefore be used to monitor ROS production/consumption over longer time periods (Woolley et al., 2013). Within this set of probes, reduction-oxidation-sensitive GFPs (roGFP) are ratiometric, dual-excitation reporters (excitation 395/470 nm, emission ~510 nm), whose fluorescence intensity is sensitive to the thiol redox potential (Hanson et al., 2004). In addition to their ratiometric measurements, roGFP probes are favoured over the redox-sensitive YFP reporters (rxYFP, (Ostergaard et al., 2001)) as they have higher redox sensitivity and lower pH sensitivity (Tantama et al., 2012, Booth et al., 2016). roGFP has been targeted to neuronal mitochondria *in vitro* and *in vivo* (mito-roGFP/roGFPm) (Guzman et al., 2010, Wagener et al., 2016). A roGFP variant with Glutaredoxin-1 fused to roGFP (Grx1-roGFP2) reports the glutathione redox potential (Gutscher et al., 2008, Breckwoldt et al., 2014), and roGFP2-Tsa1/2 are peroxiredoxin-based sensors of H_2O_2, although they remain to be tested in mammals (Morgan et al., 2016). HyPer is another roGFP variant specifically sensitive to H_2O_2 (Belousov et al., 2006), but comprises a strongly pH-sensitive cpYFP, limiting its utility (De Michele et al., 2014, Tantama et al., 2012).

Table 7: Several fluorescent reporters of reactive oxygen species (ROS) that have been successfully targeted to neuronal mitochondria. These reporters do not have absolute specificity for any single ROS type, and the accurate measurement of mitochondria-derived ROS is associated with various drawbacks, as outlined in the text. Publications refer to the work that originally generated the probe and/or studies where the probe was utilised in neuronal mitochondria.

Reporter name	**Reporter type**	**Peak excitation, emission wavelengths (nm)**	**References**
mito-HEt **MitoSOX Red**	Fluorescent molecule	λ_{ex} ~543 λ_{em} ~585	(Abramov et al., 2007, Rueda et al., 2015)
MitoPY1	Fluorescein/rhodamine fluorescent molecule	λ_{ex} ~510 λ_{em} ~528	(Dickinson et al., 2013, Duregotti et al., 2015)
mito-roGFP **roGFPm**	Single FP (dual-excitation, ratiometric)	λ_{ex} ~395, ~470 λ_{em} ~510	(Hanson et al., 2004, Guzman et al., 2010,

			Wagener et al., 2016)
Mito-Grx1-roGFP2	Single FP (dual-excitation, ratiometric)	λ_{ex} ~395, ~488 λ_{em} ~510	(Gutscher et al., 2008, Breckwoldt et al., 2016)

Redox-sensitive enzymatic assays

Spectrophotometric enzymatic assays have historically been the workhorse assays of traditional biochemists studying redox biology, but in contrast to fluorescence measurements, these assays only provide fixed time-point readouts. The activity of aconitase, a TCA cycle enzyme that catalyses the isomerisation of citrate to isocitrate, is reversibly inhibited by superoxide, peroxynitrite and H_2O_2, and decreased aconitase activity is used as an indicator of increased ROS (Vincent et al., 2005, Sipos et al., 2003)). Aconitase activity spectrophotometric assays are commercially available. Aconitase can also be a source of ROS (Sipos et al., 2003), however, and cytosolic aconitase (mRNA binding regulator of iron homeostasis) contributes ~15-25 % of total cellular aconitase activity (Liang et al., 2000).

6. Additional considerations

We address here, in a non-exhaustive list, some points worth considering when investigating mitochondrial function, with particular relevance to the methods discussed in this article.

- It is vital to select indicators with affinities/dissociation constants and dynamic ranges appropriate for the desired measurement, and to optimise drug concentrations in each experimental setting. Generally, concentrations between 0.1-10 times the reporter's K_d can be measured most reliably.
- A useful resource for experiment design utilising fluorescent reporters is provided by ThermoFisher Scientific, which displays the single-photon excitation and emission spectra of a broad array of (commercially available) fluorescent indicators - *https://www.thermofisher.com/ie/en/home/life-science/cell-analysis/labeling-chemistry/fluorescence-spectraviewer.html*. It is important to ensure minimal spectral overlap if utilising multiple fluorophores simultaneously.
- Fluorescent dyes should generally be allowed to equilibrate within cells for at least 30 min prior to imaging, and up to 60 min if required – the signal can be measured to ensure it has reached a steady state. Removal of potential-sensitive dye can lead to re-equilibration of the dye across the cell membranes, altering signal intensity. Appropriate baseline and light control experiments should be performed to verify equilibration as well as to ensure signal stability and avoid artefacts (focal-drift, phototoxicity etc.).
- Saturation of fluorescent signal should be avoided and settings should be optimised at the beginning of experiments to allow for the anticipated range of fluorescent signal fluctuations. On this note, optimised microscope settings should remain constant for all similar experiments, to enable inter-experiment comparison.
- Temperature can significantly alter neuronal physiology and assay performance. The affinity of the ATeam fluorescent reporter of ATP concentration, for instance, can vary five-fold over a temperature range of 10 °C (Imamura et al., 2009). Where possible, experiments should be carried out at the physiological 37 °C.
- Bioenergetic parameters are exceptionally sensitive (particularly at steady-state), and experimental measurements may themselves alter intracellular conditions and physiology. For instance, the relatively large GFP molecule may impact mitochondrial transport, and many indicators also act as buffers of the species they are measuring, potentially disrupting physiological dynamics. For this and other reasons, it is good practice to verify results with complementary techniques.
- Positive and negative controls and appropriate data normalisation are, as with all experiments, critical for correct interpretation of results.

- Steady-state values (e.g. metabolite or ion concentrations, pH) indicate the balance between the generation/influx and the destruction/metabolism/efflux of the measured component. Direct measurements of steady-state values provide no information on these specific processes, and further experiments are required to elucidate the contributing mechanisms.
- Changes in mitochondrial morphology or number (e.g. due to fission/fusion, biogenesis or mitophagy) can impact mitochondrial parameters measured at the whole cell level, and should ideally be monitored in conjunction with any investigation of mitochondrial bioenergetic function.

7. Conclusions

In this consensus article we have provided detailed guidelines for the thorough investigation of essential mitochondrial bioenergetic function in cellular models of neurodegenerative diseases, including specific protocols for the measurement of oxygen consumption rate in intact primary neurons, and single-neuron time-lapse fluorescence imaging of the mitochondrial membrane potential and mitochondrial NAD(P)H. These guidelines facilitate analysis of primary and secondary mitochondrial dysfunction in neurodegenerative diseases. Adherence to standardised protocols will enable experimental comparison between laboratories, consolidating this vast area of research and optimising translation of *in vitro* findings to *in vivo* studies.

8. Abbreviations

$\Delta\psi_m$	Mitochondrial membrane potential	HPLC	High performance liquid chromatography
$\Delta\psi_p$	Plasma membrane potential	iPSC	Induced pluripotent stem cell
AD	Alzheimer's disease	MDR	Multidrug resistance
ALS	Amyotrophic lateral sclerosis	ND	Neurodegenerative disease
ANT	Adenine nucleotide translocator	NPC	Neural progenitor cell
BRET	Bioluminescence energy transfer	O_2	Oxygen
Ca^{2+}	Calcium	OCR	Oxygen consumption rate
CaM	Calmodulin	OxPhos	Oxidative phosphorylation
CFP	Cyan fluorescent protein	PD	Parkinson's disease
FRET	Förster resonance energy transfer	ROS	Reactive oxygen species
FP	Fluorescent protein	TCA	Tricarboxylic acid
GFP	Green fluorescent protein	TMRM	Tetramethylrhodamine methyl ester
HD	Huntington's disease	YFP	Yellow fluorescent protein

9. Acknowledgements

We acknowledge the support of the CeBioND EU Joint Programme for Neurodegenerative Disease Research (JPND; www.jpnd.eu). The programme is supported through the following national funding organisations: Canada, CIHR; Germany, BMBF; Ireland: Science Foundation Ireland (14/JPND/ B3077); Italy: MIUR; Sweden: VS.

10. Conflict of Interest

The authors declare no conflict of interest.

11. References

ABAD, M. F., DI BENEDETTO, G., MAGALHAES, P. J., FILIPPIN, L. & POZZAN, T. 2004. Mitochondrial pH monitored by a new engineered green fluorescent protein mutant. *J Biol Chem,* 279**,** 11521-9.

ABRAMOV, A. Y., SCORZIELLO, A. & DUCHEN, M. R. 2007. Three distinct mechanisms generate oxygen free radicals in neurons and contribute to cell death during anoxia and reoxygenation. *J Neurosci,* 27**,** 1129-38.

ADAM-VIZI, V. & CHINOPOULOS, C. 2006. Bioenergetics and the formation of mitochondrial reactive oxygen species. *Trends Pharmacol Sci,* 27**,** 639-45.

AKERBOOM, J., CARRERAS CALDERON, N., TIAN, L., WABNIG, S., PRIGGE, M., TOLO, J., GORDUS, A., ORGER, M. B., SEVERI, K. E., MACKLIN, J. J., PATEL, R., PULVER, S. R., WARDILL, T. J., FISCHER, E., SCHULER, C., CHEN, T. W., SARKISYAN, K. S., MARVIN, J. S., BARGMANN, C. I., KIM, D. S., KUGLER, S., LAGNADO, L., HEGEMANN, P., GOTTSCHALK, A., SCHREITER, E. R. & LOOGER, L. L. 2013. Genetically encoded calcium indicators for multi-color neural activity imaging and combination with optogenetics. *Front Mol Neurosci,* 6**,** 2.

AOUACHERIA, A., BAGHDIGUIAN, S., LAMB, H. M., HUSKA, J. D., PINEDA, F. J. & HARDWICK, J. M. 2017. Connecting mitochondrial dynamics and life-or-death events via Bcl-2 family proteins. *Neurochem Int*.

BARRIENTOS, A., FONTANESI, F. & DIAZ, F. 2009. Evaluation of the mitochondrial respiratory chain and oxidative phosphorylation system using polarography and spectrophotometric enzyme assays. *Curr Protoc Hum Genet,* Chapter 19**,** Unit19 3.

BARSUKOVA, A. G., BOURDETTE, D. & FORTE, M. 2011. Mitochondrial calcium and its regulation in neurodegeneration induced by oxidative stress. *Eur J Neurosci,* 34**,** 437-47.

BELOUSOV, V. V., FRADKOV, A. F., LUKYANOV, K. A., STAROVEROV, D. B., SHAKHBAZOV, K. S., TERSKIKH, A. V. & LUKYANOV, S. 2006. Genetically encoded fluorescent indicator for intracellular hydrogen peroxide. *Nat Methods,* 3**,** 281-6.

BENCINA, M. 2013. Illumination of the spatial order of intracellular pH by genetically encoded pH-sensitive sensors. *Sensors (Basel),* 13**,** 16736-58.

BERG, J., HUNG, Y. P. & YELLEN, G. 2009. A genetically encoded fluorescent reporter of ATP:ADP ratio. *Nat Methods,* 6**,** 161-6.

BERNARDI, P., PETRONILLI, V., DI LISA, F. & FORTE, M. 2001. A mitochondrial perspective on cell death. *Trends Biochem Sci,* 26**,** 112-7.

BEZPROZVANNY, I. & MATTSON, M. P. 2008. Neuronal calcium mishandling and the pathogenesis of Alzheimer's disease. *Trends Neurosci,* 31**,** 454-63.

BIFFI, E., REGALIA, G., MENEGON, A., FERRIGNO, G. & PEDROCCHI, A. 2013. The influence of neuronal density and maturation on network activity of hippocampal cell cultures: a methodological study. *PLoS One,* 8**,** e83899.

BILAN, D. S. & BELOUSOV, V. V. 2016. Genetically encoded probes for NAD+/NADH monitoring. *Free Radic Biol Med,* 100**,** 32-42.

BILAN, D. S., MATLASHOV, M. E., GOROKHOVATSKY, A. Y., SCHULTZ, C., ENIKOLOPOV, G. & BELOUSOV, V. V. 2014. Genetically encoded fluorescent indicator for imaging NAD(+)/NADH ratio changes in different cellular compartments. *Biochim Biophys Acta,* 1840**,** 951-7.

BINDOKAS, V. P., JORDAN, J., LEE, C. C. & MILLER, R. J. 1996. Superoxide production in rat hippocampal neurons: selective imaging with hydroethidine. *J Neurosci,* 16**,** 1324-36.

BIZAT, N., GALAS, M. C., JACQUARD, C., BOYER, F., HERMEL, J. M., SCHIFFMANN, S. N., HANTRAYE, P., BLUM, D. & BROUILLET, E. 2005. Neuroprotective effect of zVAD against the neurotoxin 3-nitropropionic acid involves inhibition of calpain. *Neuropharmacology,* 49**,** 695-702.

BLACKER, T. S., BERECZ, T., DUCHEN, M. R. & SZABADKAI, G. 2017. Assessment of Cellular Redox State Using NAD(P)H Fluorescence Intensity and Lifetime. *Bio Protoc,* 7.

BLACKER, T. S. & DUCHEN, M. R. 2016. Investigating mitochondrial redox state using NADH and NADPH autofluorescence. *Free Radic Biol Med,* 100**,** 53-65.

BOLSHAKOV, A. P., MIKHAILOVA, M. M., SZABADKAI, G., PINELIS, V. G., BRUSTOVETSKY, N., RIZZUTO, R. & KHODOROV, B. I. 2008. Measurements of mitochondrial pH in cultured cortical neurons clarify contribution of mitochondrial pore to the mechanism of glutamate-induced delayed Ca2+ deregulation. *Cell Calcium,* 43**,** 602-14.

BONORA, M., GIORGI, C., BONONI, A., MARCHI, S., PATERGNANI, S., RIMESSI, A., RIZZUTO, R. & PINTON, P. 2013. Subcellular calcium measurements in mammalian cells using jellyfish photoprotein aequorin-based probes. *Nat Protoc,* 8**,** 2105-18.

BOOTH, D. M., JOSEPH, S. K. & HAJNOCZKY, G. 2016. Subcellular ROS imaging methods: Relevance for the study of calcium signaling. *Cell Calcium,* 60**,** 65-73.

BRAND, M. D. 2016. Mitochondrial generation of superoxide and hydrogen peroxide as the source of mitochondrial redox signaling. *Free Radic Biol Med,* 100**,** 14-31.

BRAND, M. D. & NICHOLLS, D. G. 2011. Assessing mitochondrial dysfunction in cells. *Biochem J,* 435**,** 297-312.

BRECKWOLDT, M. O., ARMOUNDAS, A. A., AON, M. A., BENDSZUS, M., O'ROURKE, B., SCHWARZLANDER, M., DICK, T. P. & KURZ, F. T. 2016. Mitochondrial redox and pH signaling occurs in axonal and synaptic organelle clusters. *Sci Rep,* 6**,** 23251.

BRECKWOLDT, M. O., PFISTER, F. M., BRADLEY, P. M., MARINKOVIC, P., WILLIAMS, P. R., BRILL, M. S., PLOMER, B., SCHMALZ, A., ST CLAIR, D. K., NAUMANN, R., GRIESBECK, O., SCHWARZLANDER, M., GODINHO, L., BAREYRE, F. M., DICK, T. P., KERSCHENSTEINER, M. & MISGELD, T. 2014. Multiparametric optical analysis of mitochondrial redox signals during neuronal physiology and pathology in vivo. *Nat Med,* 20**,** 555-60.

BRENNAN, A. M., SUH, S. W., WON, S. J., NARASIMHAN, P., KAUPPINEN, T. M., LEE, H., EDLING, Y., CHAN, P. H. & SWANSON, R. A. 2009. NADPH oxidase is the primary source of superoxide induced by NMDA receptor activation. *Nat Neurosci,* 12**,** 857-63.

BROUILLET, E., CONDE, F., BEAL, M. F. & HANTRAYE, P. 1999. Replicating Huntington's disease phenotype in experimental animals. *Prog Neurobiol,* 59**,** 427-68.

CAMBRONNE, X. A., STEWART, M. L., KIM, D., JONES-BRUNETTE, A. M., MORGAN, R. K., FARRENS, D. L., COHEN, M. S. & GOODMAN, R. H. 2016. Biosensor reveals multiple sources for mitochondrial NAD(+). *Science,* 352**,** 1474-7.

CAN, K., KÜGLER, S. & MÜLLER, M. 2017. Live Imaging of Mitochondrial ROS Production and Dynamic Redox Balance in Neurons. *In:* STRACK, S. & USACHEV, Y. M. (eds.) *Techniques to Investigate Mitochondrial Function in Neurons.* New York, NY: Springer New York.

CHACKO, B. K., KRAMER, P. A., RAVI, S., BENAVIDES, G. A., MITCHELL, T., DRANKA, B. P., FERRICK, D., SINGAL, A. K., BALLINGER, S. W., BAILEY, S. M., HARDY, R. W., ZHANG, J., ZHI, D. & DARLEY-USMAR, V. M. 2014. The Bioenergetic Health Index: a new concept in mitochondrial translational research. *Clin Sci (Lond),* 127**,** 367-73.

CHAKRABORTY, S., NIAN, F. S., TSAI, J. W., KARMENYAN, A. & CHIOU, A. 2016. Quantification of the Metabolic State in Cell-Model of Parkinson's Disease by Fluorescence Lifetime Imaging Microscopy. *Sci Rep,* 6**,** 19145.

CHANCE, B. 1962. Kinetics of enzyme reactions within single cells. *Ann N Y Acad Sci,* 97**,** 431-48.

CHEN, M., WANG, Y., HOU, T., ZHANG, H., QU, A. & WANG, X. 2011. Differential mitochondrial calcium responses in different cell types detected with a mitochondrial calcium fluorescent indicator, mito-GCaMP2. *Acta Biochim Biophys Sin (Shanghai),* 43**,** 822-30.

CHEN, X., ZHONG, Z., XU, Z., CHEN, L. & WANG, Y. 2010. 2',7'-Dichlorodihydrofluorescein as a fluorescent probe for reactive oxygen species measurement: Forty years of application and controversy. *Free Radic Res,* 44**,** 587-604.

CHINOPOULOS, C., GERENCSER, A. A., MANDI, M., MATHE, K., TOROCSIK, B., DOCZI, J., TURIAK, L., KISS, G., KONRAD, C., VAJDA, S., VERECZKI, V., OH, R. J. & ADAM-VIZI, V. 2010. Forward operation of adenine nucleotide translocase during F0F1-ATPase reversal: critical role of matrix substrate-level phosphorylation. *FASEB J,* 24**,** 2405-16.

CHINOPOULOS, C., KISS, G., KAWAMATA, H. & STARKOV, A. A. 2014. Measurement of ADP-ATP exchange in relation to mitochondrial transmembrane potential and oxygen consumption. *Methods Enzymol,* 542**,** 333-48.

CHOI, S. H., KIM, Y. H., QUINTI, L., TANZI, R. E. & KIM, D. Y. 2016. 3D culture models of Alzheimer's disease: a road map to a "cure-in-a-dish". *Mol Neurodegener,* 11**,** 75.

CLERC, P. & POLSTER, B. M. 2012. Investigation of mitochondrial dysfunction by sequential microplate-based respiration measurements from intact and permeabilized neurons. *PLoS One,* 7**,** e34465.

CONNOLLY, N. M., DUSSMANN, H., ANILKUMAR, U., HUBER, H. J. & PREHN, J. H. 2014. Single-cell imaging of bioenergetic responses to neuronal excitotoxicity and oxygen and glucose deprivation. *J Neurosci,* 34**,** 10192-205.

CONNOLLY, N. M. & PREHN, J. H. 2015. The metabolic response to excitotoxicity - lessons from single-cell imaging. *Journal of bioenergetics and biomembranes,* 47**,** 75-88.

CONSTANTINESCU, R., CONSTANTINESCU, A. T., REICHMANN, H. & JANETZKY, B. 2007. Neuronal differentiation and long-term culture of the human neuroblastoma line SH-SY5Y. *J Neural Transm Suppl***,** 17-28.

DE MICHELE, R., CARIMI, F. & FROMMER, W. B. 2014. Mitochondrial biosensors. *Int J Biochem Cell Biol,* 48**,** 39-44.

DE STEFANI, D., RIZZUTO, R. & POZZAN, T. 2016. Enjoy the Trip: Calcium in Mitochondria Back and Forth. *Annu Rev Biochem,* 85**,** 161-92.

DICKINSON, B. C., LIN, V. S. & CHANG, C. J. 2013. Preparation and use of MitoPY1 for imaging hydrogen peroxide in mitochondria of live cells. *Nat Protoc,* 8**,** 1249-59.

DICKINSON, B. C., SRIKUN, D. & CHANG, C. J. 2010. Mitochondrial-targeted fluorescent probes for reactive oxygen species. *Curr Opin Chem Biol,* 14**,** 50-6.

DMITRIEV, R. I., BORISOV, S. M., KONDRASHINA, A. V., PAKAN, J. M., ANILKUMAR, U., PREHN, J. H., ZHDANOV, A. V., MCDERMOTT, K. W., KLIMANT, I. & PAPKOVSKY, D. B. 2015. Imaging oxygen in neural cell and tissue models by means of anionic cell-permeable phosphorescent nanoparticles. *Cell Mol Life Sci,* 72**,** 367-81.

DRANKA, B. P., BENAVIDES, G. A., DIERS, A. R., GIORDANO, S., ZELICKSON, B. R., REILY, C., ZOU, L., CHATHAM, J. C., HILL, B. G., ZHANG, J., LANDAR, A. & DARLEY-USMAR, V. M. 2011. Assessing bioenergetic function in response to oxidative stress by metabolic profiling. *Free Radic Biol Med,* 51**,** 1621-35.

DUAN, W., GUO, Z. & MATTSON, M. P. 2000. Participation of par-4 in the degeneration of striatal neurons induced by metabolic compromise with 3-nitropropionic acid. *Exp Neurol,* 165**,** 1-11.

DUGAN, L. L., SENSI, S. L., CANZONIERO, L. M., HANDRAN, S. D., ROTHMAN, S. M., LIN, T. S., GOLDBERG, M. P. & CHOI, D. W. 1995. Mitochondrial production of reactive oxygen species in cortical neurons following exposure to N-methyl-D-aspartate. *J Neurosci,* 15**,** 6377-88.

DUREGOTTI, E., NEGRO, S., SCORZETO, M., ZORNETTA, I., DICKINSON, B. C., CHANG, C. J., MONTECUCCO, C. & RIGONI, M. 2015. Mitochondrial alarmins released by degenerating motor axon terminals activate perisynaptic Schwann cells. *Proc Natl Acad Sci U S A,* 112**,** E497-505.

FAIRBANKS, S. L., VEST, R., VERMA, S., TRAYSTMAN, R. J. & HERSON, P. S. 2013. Sex stratified neuronal cultures to study ischemic cell death pathways. *J Vis Exp***,** e50758.

FANG, E. F., SCHEIBYE-KNUDSEN, M., CHUA, K. F., MATTSON, M. P., CROTEAU, D. L. & BOHR, V. A. 2016. Nuclear DNA damage signalling to mitochondria in ageing. *Nat Rev Mol Cell Biol,* 17**,** 308-21.

GAO, J., WANG, L., LIU, J., XIE, F., SU, B. & WANG, X. 2017. Abnormalities of Mitochondrial Dynamics in Neurodegenerative Diseases. *Antioxidants (Basel),* 6.

GARCIA, O., ALMEIDA, A., MASSIEU, L. & BOLANOS, J. P. 2005. Increased mitochondrial respiration maintains the mitochondrial membrane potential and promotes survival of cerebellar neurons in an endogenous model of glutamate receptor activation. *J Neurochem,* 92**,** 183-90.

GERENCSER, A. A., CHINOPOULOS, C., BIRKET, M. J., JASTROCH, M., VITELLI, C., NICHOLLS, D. G. & BRAND, M. D. 2012. Quantitative measurement of mitochondrial

membrane potential in cultured cells: calcium-induced de- and hyperpolarization of neuronal mitochondria. *J Physiol,* 590**,** 2845-71.

GOTZ, J. & ITTNER, L. M. 2008. Animal models of Alzheimer's disease and frontotemporal dementia. *Nat Rev Neurosci,* 9**,** 532-44.

GREENE, L. A. & TISCHLER, A. S. 1976. Establishment of a noradrenergic clonal line of rat adrenal pheochromocytoma cells which respond to nerve growth factor. *Proc Natl Acad Sci U S A,* 73**,** 2424-8.

GRIENBERGER, C. & KONNERTH, A. 2012. Imaging calcium in neurons. *Neuron,* 73**,** 862-85.

GUTSCHER, M., PAULEAU, A. L., MARTY, L., BRACH, T., WABNITZ, G. H., SAMSTAG, Y., MEYER, A. J. & DICK, T. P. 2008. Real-time imaging of the intracellular glutathione redox potential. *Nat Methods,* 5**,** 553-9.

GUZMAN, J. N., SANCHEZ-PADILLA, J., WOKOSIN, D., KONDAPALLI, J., ILIJIC, E., SCHUMACKER, P. T. & SURMEIER, D. J. 2010. Oxidant stress evoked by pacemaking in dopaminergic neurons is attenuated by DJ-1. *Nature,* 468**,** 696-700.

HANSON, G. T., AGGELER, R., OGLESBEE, D., CANNON, M., CAPALDI, R. A., TSIEN, R. Y. & REMINGTON, S. J. 2004. Investigating mitochondrial redox potential with redox-sensitive green fluorescent protein indicators. *J Biol Chem,* 279**,** 13044-53.

HARPUR, A. G., WOUTERS, F. S. & BASTIAENS, P. I. 2001. Imaging FRET between spectrally similar GFP molecules in single cells. *Nat Biotechnol,* 19**,** 167-9.

HARVEY, B. K., RICHIE, C. T., HOFFER, B. J. & AIRAVAARA, M. 2011. Transgenic animal models of neurodegeneration based on human genetic studies. *J Neural Transm (Vienna),* 118**,** 27-45.

HAYAKAWA, Y., NEMOTO, T., IINO, M. & KASAI, H. 2005. Rapid Ca2+-dependent increase in oxygen consumption by mitochondria in single mammalian central neurons. *Cell Calcium,* 37**,** 359-70.

HEMPEL, S. L., BUETTNER, G. R., O'MALLEY, Y. Q., WESSELS, D. A. & FLAHERTY, D. M. 1999. Dihydrofluorescein diacetate is superior for detecting intracellular oxidants: comparison with 2',7'-dichlorodihydrofluorescein diacetate, 5(and 6)-carboxy-2',7'-dichlorodihydrofluorescein diacetate, and dihydrorhodamine 123. *Free Radic Biol Med,* 27**,** 146-59.

HERRERO-MENDEZ, A., ALMEIDA, A., FERNANDEZ, E., MAESTRE, C., MONCADA, S. & BOLANOS, J. P. 2009. The bioenergetic and antioxidant status of neurons is controlled by continuous degradation of a key glycolytic enzyme by APC/C-Cdh1. *Nat Cell Biol,* 11**,** 747-52.

HILGENBERG, L. G. & SMITH, M. A. 2007. Preparation of dissociated mouse cortical neuron cultures. *J Vis Exp***,** 562.

HORAN, M. P., PICHAUD, N. & BALLARD, J. W. 2012. Review: quantifying mitochondrial dysfunction in complex diseases of aging. *J Gerontol A Biol Sci Med Sci,* 67**,** 1022-35.

HUANG, S., HEIKAL, A. A. & WEBB, W. W. 2002. Two-photon fluorescence spectroscopy and microscopy of NAD(P)H and flavoprotein. *Biophys J,* 82**,** 2811-25.

HUNG, S. S., KHAN, S., LO, C. Y., HEWITT, A. W. & WONG, R. C. 2017. Drug discovery using induced pluripotent stem cell models of neurodegenerative and ocular diseases. *Pharmacol Ther*.

HUNG, Y. P., ALBECK, J. G., TANTAMA, M. & YELLEN, G. 2011. Imaging cytosolic NADH-NAD(+) redox state with a genetically encoded fluorescent biosensor. *Cell Metabolism,* 14**,** 545-54.

IMAMURA, H., NHAT, K. P., TOGAWA, H., SAITO, K., IINO, R., KATO-YAMADA, Y., NAGAI, T. & NOJI, H. 2009. Visualization of ATP levels inside single living cells with fluorescence resonance energy transfer-based genetically encoded indicators. *Proc Natl Acad Sci U S A,* 106**,** 15651-6.

IRWIN, W. A., BERGAMIN, N., SABATELLI, P., REGGIANI, C., MEGIGHIAN, A., MERLINI, L., BRAGHETTA, P., COLUMBARO, M., VOLPIN, D., BRESSAN, G. M., BERNARDI, P. & BONALDO, P. 2003. Mitochondrial dysfunction and apoptosis in myopathic mice with collagen VI deficiency. *Nat Genet,* 35**,** 367-71.

JASTROCH, M., DIVAKARUNI, A. S., MOOKERJEE, S., TREBERG, J. R. & BRAND, M. D. 2010. Mitochondrial proton and electron leaks. *Essays Biochem,* 47**,** 53-67.

JEKABSONS, M. B. & NICHOLLS, D. G. 2004. In situ respiration and bioenergetic status of mitochondria in primary cerebellar granule neuronal cultures exposed continuously to glutamate. *J Biol Chem,* 279**,** 32989-3000.

JOHRI, A. & BEAL, M. F. 2012. Mitochondrial dysfunction in neurodegenerative diseases. *J Pharmacol Exp Ther,* 342**,** 619-30.

JOSHI, D. C. & BAKOWSKA, J. C. 2011. Determination of mitochondrial membrane potential and reactive oxygen species in live rat cortical neurons. *J Vis Exp*.

JUNG, C., HIGGINS, C. M. & XU, Z. 2000. Measuring the quantity and activity of mitochondrial electron transport chain complexes in tissues of central nervous system using blue native polyacrylamide gel electrophoresis. *Anal Biochem,* 286**,** 214-23.

KAHRAMAN, S., SIEGEL, A., POLSTER, B. M. & FISKUM, G. 2015. Permeability transition pore-dependent and PARP-mediated depletion of neuronal pyridine nucleotides during anoxia and glucose deprivation. *J Bioenerg Biomembr,* 47**,** 53-61.

KANN, O. & KOVACS, R. 2007. Mitochondria and neuronal activity. *Am J Physiol Cell Physiol,* 292**,** C641-57.

KARRA, D. & DAHM, R. 2010. Transfection techniques for neuronal cells. *J Neurosci,* 30**,** 6171-7.

KASISCHKE, K. A., VISHWASRAO, H. D., FISHER, P. J., ZIPFEL, W. R. & WEBB, W. W. 2004. Neural activity triggers neuronal oxidative metabolism followed by astrocytic glycolysis. *Science,* 305**,** 99-103.

KATSURA, K., RODRIGUEZ DE TURCO, E. B., FOLBERGROVA, J., BAZAN, N. G. & SIESJO, B. K. 1993. Coupling among energy failure, loss of ion homeostasis, and phospholipase A2 and C activation during ischemia. *J Neurochem,* 61**,** 1677-84.

KLEMAN, A. M., YUAN, J. Y., AJA, S., RONNETT, G. V. & LANDREE, L. E. 2008. Physiological glucose is critical for optimized neuronal viability and AMPK responsiveness in vitro. *J Neurosci Methods,* 167**,** 292-301.

KONDRASHINA, A. V., OGURTSOV, V. I. & PAPKOVSKY, D. B. 2015. Comparison of the three optical platforms for measurement of cellular respiration. *Anal Biochem,* 468**,** 1-3.

LEPAGE, K. T., DICKEY, R. W., GERWICK, W. H., JESTER, E. L. & MURRAY, T. F. 2005. On the use of neuro-2a neuroblastoma cells versus intact neurons in primary culture for neurotoxicity studies. *Crit Rev Neurobiol,* 17**,** 27-50.

LEWIS, C. A., PARKER, S. J., FISKE, B. P., MCCLOSKEY, D., GUI, D. Y., GREEN, C. R., VOKES, N. I., FEIST, A. M., VANDER HEIDEN, M. G. & METALLO, C. M. 2014. Tracing compartmentalized NADPH metabolism in the cytosol and mitochondria of mammalian cells. *Mol Cell,* 55**,** 253-63.

LI, Y. & TSIEN, R. W. 2012. pHTomato, a red, genetically encoded indicator that enables multiplex interrogation of synaptic activity. *Nat Neurosci,* 15**,** 1047-53.

LIANG, L. P., HO, Y. S. & PATEL, M. 2000. Mitochondrial superoxide production in kainate-induced hippocampal damage. *Neuroscience,* 101**,** 563-70.

LIN, M. T. & BEAL, M. F. 2006. Mitochondrial dysfunction and oxidative stress in neurodegenerative diseases. *Nature,* 443**,** 787-95.

LLORENTE-FOLCH, I., RUEDA, C. B., AMIGO, I., DEL ARCO, A., SAHEKI, T., PARDO, B. & SATRUSTEGUI, J. 2013. Calcium-regulation of mitochondrial respiration maintains ATP homeostasis and requires ARALAR/AGC1-malate aspartate shuttle in intact cortical neurons. *J Neurosci,* 33**,** 13957-71, 13971a.

LLORENTE-FOLCH, I., RUEDA, C. B., PARDO, B., SZABADKAI, G., DUCHEN, M. R. & SATRUSTEGUI, J. 2015. The regulation of neuronal mitochondrial metabolism by calcium. *J Physiol,* 593**,** 3447-62.

LOPEZ-FABUEL, I., LE DOUCE, J., LOGAN, A., JAMES, A. M., BONVENTO, G., MURPHY, M. P., ALMEIDA, A. & BOLANOS, J. P. 2016. Complex I assembly into supercomplexes determines differential mitochondrial ROS production in neurons and astrocytes. *Proc Natl Acad Sci U S A,* 113**,** 13063-13068.

MARTINEZ, T. N. & GREENAMYRE, J. T. 2012. Toxin models of mitochondrial dysfunction in Parkinson's disease. *Antioxid Redox Signal,* 16**,** 920-34.

MIESENBOCK, G., DE ANGELIS, D. A. & ROTHMAN, J. E. 1998. Visualizing secretion and synaptic transmission with pH-sensitive green fluorescent proteins. *Nature,* 394**,** 192-5.
MITCHELL, P. & MOYLE, J. 1969. Estimation of membrane potential and pH difference across the cristae membrane of rat liver mitochondria. *Eur J Biochem,* 7**,** 471-84.
MIYAWAKI, A., GRIESBECK, O., HEIM, R. & TSIEN, R. Y. 1999. Dynamic and quantitative Ca2+ measurements using improved cameleons. *Proc Natl Acad Sci U S A,* 96**,** 2135-40.
MOOKERJEE, S. A., GERENCSER, A. A., NICHOLLS, D. G. & BRAND, M. D. 2017. Quantifying intracellular rates of glycolytic and oxidative ATP production and consumption using extracellular flux measurements. *J Biol Chem,* 292**,** 7189-7207.
MOOKERJEE, S. A., GONCALVES, R. L., GERENCSER, A. A., NICHOLLS, D. G. & BRAND, M. D. 2015. The contributions of respiration and glycolysis to extracellular acid production. *Biochim Biophys Acta,* 1847**,** 171-81.
MOOKERJEE, S. A., NICHOLLS, D. G. & BRAND, M. D. 2016. Determining Maximum Glycolytic Capacity Using Extracellular Flux Measurements. *PLoS One,* 11**,** e0152016.
MORGAN, B., VAN LAER, K., OWUSU, T. N., EZERINA, D., PASTOR-FLORES, D., AMPONSAH, P. S., TURSCH, A. & DICK, T. P. 2016. Real-time monitoring of basal H2O2 levels with peroxiredoxin-based probes. *Nat Chem Biol,* 12**,** 437-43.
MURPHY, M. P. 2009. How mitochondria produce reactive oxygen species. *Biochem J,* 417**,** 1-13.
MURPHY, M. P., HOLMGREN, A., LARSSON, N. G., HALLIWELL, B., CHANG, C. J., KALYANARAMAN, B., RHEE, S. G., THORNALLEY, P. J., PARTRIDGE, L., GEMS, D., NYSTROM, T., BELOUSOV, V., SCHUMACKER, P. T. & WINTERBOURN, C. C. 2011. Unraveling the biological roles of reactive oxygen species. *Cell Metab,* 13**,** 361-6.
NAGAI, T., SAWANO, A., PARK, E. S. & MIYAWAKI, A. 2001. Circularly permuted green fluorescent proteins engineered to sense Ca2+. *Proc Natl Acad Sci U S A,* 98**,** 3197-202.
NAGAI, T., YAMADA, S., TOMINAGA, T., ICHIKAWA, M. & MIYAWAKI, A. 2004. Expanded dynamic range of fluorescent indicators for Ca(2+) by circularly permuted yellow fluorescent proteins. *Proc Natl Acad Sci U S A,* 101**,** 10554-9.
NAKAI, J., OHKURA, M. & IMOTO, K. 2001. A high signal-to-noise Ca(2+) probe composed of a single green fluorescent protein. *Nat Biotechnol,* 19**,** 137-41.
NAKANO, M., IMAMURA, H., NAGAI, T. & NOJI, H. 2011. Ca(2)(+) regulation of mitochondrial ATP synthesis visualized at the single cell level. *ACS Chem Biol,* 6**,** 709-15.
NICHOLLS, D. G. 2006. Simultaneous monitoring of ionophore- and inhibitor-mediated plasma and mitochondrial membrane potential changes in cultured neurons. *J Biol Chem,* 281**,** 14864-74.
NICHOLLS, D. G. & BUDD, S. L. 2000. Mitochondria and neuronal survival. *Physiol Rev,* 80**,** 315-60.
NICHOLLS, D. G. & FERGUSON, S. 2013. *Bioenergetics*, Academic Press.
OGIKUBO, S., NAKABAYASHI, T., ADACHI, T., ISLAM, M. S., YOSHIZAWA, T., KINJO, M. & OHTA, N. 2011. Intracellular pH sensing using autofluorescence lifetime microscopy. *J Phys Chem B,* 115**,** 10385-90.
OSTERGAARD, H., HENRIKSEN, A., HANSEN, F. G. & WINTHER, J. R. 2001. Shedding light on disulfide bond formation: engineering a redox switch in green fluorescent protein. *EMBO J,* 20**,** 5853-62.
PALMER, A. E., GIACOMELLO, M., KORTEMME, T., HIRES, S. A., LEV-RAM, V., BAKER, D. & TSIEN, R. Y. 2006. Ca2+ indicators based on computationally redesigned calmodulin-peptide pairs. *Chem Biol,* 13**,** 521-30.
PALTY, R., SILVERMAN, W. F., HERSHFINKEL, M., CAPORALE, T., SENSI, S. L., PARNIS, J., NOLTE, C., FISHMAN, D., SHOSHAN-BARMATZ, V., HERRMANN, S., KHANANSHVILI, D. & SEKLER, I. 2010. NCLX is an essential component of mitochondrial Na+/Ca2+ exchange. *Proc Natl Acad Sci U S A,* 107**,** 436-41.
PARDO, B., CONTRERAS, L., SERRANO, A., RAMOS, M., KOBAYASHI, K., IIJIMA, M., SAHEKI, T. & SATRUSTEGUI, J. 2006. Essential role of aralar in the transduction of small Ca2+ signals to neuronal mitochondria. *J Biol Chem,* 281**,** 1039-47.
PATHAK, D., BERTHET, A. & NAKAMURA, K. 2013. Energy failure: does it contribute to neurodegeneration? *Ann Neurol,* 74**,** 506-16.

PENDIN, D., GREOTTI, E., FILADI, R. & POZZAN, T. 2015. Spying on organelle Ca(2)(+) in living cells: the mitochondrial point of view. *J Endocrinol Invest,* 38**,** 39-45.

PERRY, S. W., NORMAN, J. P., BARBIERI, J., BROWN, E. B. & GELBARD, H. A. 2011. Mitochondrial membrane potential probes and the proton gradient: a practical usage guide. *BioTechniques,* 50**,** 98-115.

PIVOVAROVA, N. B. & ANDREWS, S. B. 2010. Calcium-dependent mitochondrial function and dysfunction in neurons. *FEBS J,* 277**,** 3622-36.

POBURKO, D., SANTO-DOMINGO, J. & DEMAUREX, N. 2011. Dynamic regulation of the mitochondrial proton gradient during cytosolic calcium elevations. *The Journal of Biological Chemistry,* 286**,** 11672-84.

POLSTER, B. M., NICHOLLS, D. G., GE, S. X. & ROELOFS, B. A. 2014. Use of potentiometric fluorophores in the measurement of mitochondrial reactive oxygen species. *Methods Enzymol,* 547**,** 225-50.

POLYZOS, A. A. & MCMURRAY, C. T. 2017. The chicken or the egg: mitochondrial dysfunction as a cause or consequence of toxicity in Huntington's disease. *Mech Ageing Dev,* 161**,** 181-197.

PORCELLI, A. M., GHELLI, A., ZANNA, C., PINTON, P., RIZZUTO, R. & RUGOLO, M. 2005. pH difference across the outer mitochondrial membrane measured with a green fluorescent protein mutant. *Biochem Biophys Res Commun,* 326**,** 799-804.

POZZAN, T. & RUDOLF, R. 2009. Measurements of mitochondrial calcium in vivo. *Biochim Biophys Acta,* 1787**,** 1317-23.

QIU, J., TAN, Y. W., HAGENSTON, A. M., MARTEL, M. A., KNEISEL, N., SKEHEL, P. A., WYLLIE, D. J., BADING, H. & HARDINGHAM, G. E. 2013. Mitochondrial calcium uniporter Mcu controls excitotoxicity and is transcriptionally repressed by neuroprotective nuclear calcium signals. *Nat Comms,* 4**,** 2034.

RAEFSKY, S. M. & MATTSON, M. P. 2017. Adaptive responses of neuronal mitochondria to bioenergetic challenges: Roles in neuroplasticity and disease resistance. *Free Radic Biol Med,* 102**,** 203-216.

RAJENDRAN, M., DANE, E., CONLEY, J. & TANTAMA, M. 2016. Imaging Adenosine Triphosphate (ATP). *Biol Bull,* 231**,** 73-84.

RHEIN, V., SONG, X., WIESNER, A., ITTNER, L. M., BAYSANG, G., MEIER, F., OZMEN, L., BLUETHMANN, H., DROSE, S., BRANDT, U., SAVASKAN, E., CZECH, C., GOTZ, J. & ECKERT, A. 2009. Amyloid-beta and tau synergistically impair the oxidative phosphorylation system in triple transgenic Alzheimer's disease mice. *Proc Natl Acad Sci U S A,* 106**,** 20057-62.

RIZZUTO, R., SIMPSON, A. W., BRINI, M. & POZZAN, T. 1992. Rapid changes of mitochondrial Ca2+ revealed by specifically targeted recombinant aequorin. *Nature,* 358**,** 325-7.

ROBINSON, K. M., JANES, M. S. & BECKMAN, J. S. 2008. The selective detection of mitochondrial superoxide by live cell imaging. *Nat Protoc,* 3**,** 941-7.

ROELOFS, B. A., GE, S. X., STUDLACK, P. E. & POLSTER, B. M. 2015. Low micromolar concentrations of the superoxide probe MitoSOX uncouple neural mitochondria and inhibit complex IV. *Free Radic Biol Med,* 86**,** 250-8.

ROSS, J. M. 2011. Visualization of mitochondrial respiratory function using cytochrome c oxidase/succinate dehydrogenase (COX/SDH) double-labeling histochemistry. *J Vis Exp***,** e3266.

RUAS, J. S., SIQUEIRA-SANTOS, E. S., AMIGO, I., RODRIGUES-SILVA, E., KOWALTOWSKI, A. J. & CASTILHO, R. F. 2016. Underestimation of the Maximal Capacity of the Mitochondrial Electron Transport System in Oligomycin-Treated Cells. *PLoS One,* 11**,** e0150967.

RUDOLF, R., MONGILLO, M., RIZZUTO, R. & POZZAN, T. 2003. Looking forward to seeing calcium. *Nat Rev Mol Cell Biol,* 4**,** 579-86.

RUEDA, C. B., TRABA, J., AMIGO, I., LLORENTE-FOLCH, I., GONZALEZ-SANCHEZ, P., PARDO, B., ESTEBAN, J. A., DEL ARCO, A. & SATRUSTEGUI, J. 2015. Mitochondrial ATP-Mg/Pi carrier SCaMC-3/Slc25a23 counteracts PARP-1-dependent fall in mitochondrial ATP caused by excitotoxic insults in neurons. *J Neurosci,* 35**,** 3566-81.

RYAN, S. D., DOLATABADI, N., CHAN, S. F., ZHANG, X., AKHTAR, M. W., PARKER, J., SOLDNER, F., SUNICO, C. R., NAGAR, S., TALANTOVA, M., LEE, B., LOPEZ, K., NUTTER, A., SHAN, B., MOLOKANOVA, E., ZHANG, Y., HAN, X., NAKAMURA, T., MASLIAH, E., YATES, J. R., 3RD, NAKANISHI, N., ANDREYEV, A. Y., OKAMOTO, S., JAENISCH, R., AMBASUDHAN, R. & LIPTON, S. A. 2013. Isogenic human iPSC Parkinson's model shows nitrosative stress-induced dysfunction in MEF2-PGC1alpha transcription. *Cell,* 155**,** 1351-64.

RYSTED, J. E., LIN, Z. & USACHEV, Y. M. 2017. Techniques for Simultaneous Mitochondrial and Cytosolic Ca2+ Imaging in Neurons. *Techniques to Investigate Mitochondrial Function in Neurons*. Springer Protocols.

SALABEI, J. K., GIBB, A. A. & HILL, B. G. 2014. Comprehensive measurement of respiratory activity in permeabilized cells using extracellular flux analysis. *Nat Protoc,* 9**,** 421-38.

SAN MARTIN, A., SOTELO-HITSCHFELD, T., LERCHUNDI, R., FERNANDEZ-MONCADA, I., CEBALLO, S., VALDEBENITO, R., BAEZA-LEHNERT, F., ALEGRIA, K., CONTRERAS-BAEZA, Y., GARRIDO-GERTER, P., ROMERO-GOMEZ, I. & BARROS, L. F. 2014. Single-cell imaging tools for brain energy metabolism: a review. *Neurophotonics,* 1**,** 011004.

SANTO-DOMINGO, J. & DEMAUREX, N. 2012. Perspectives on: SGP symposium on mitochondrial physiology and medicine: the renaissance of mitochondrial pH. *J Gen Physiol,* 139**,** 415-23.

SCADUTO, R. C., JR. & GROTYOHANN, L. W. 1999. Measurement of mitochondrial membrane potential using fluorescent rhodamine derivatives. *Biophys J,* 76**,** 469-77.

SCHLACHETZKI, J. C., SALIBA, S. W. & OLIVEIRA, A. C. 2013. Studying neurodegenerative diseases in culture models. *Rev Bras Psiquiatr,* 35 Suppl 2**,** S92-100.

SCHON, E. A. & PRZEDBORSKI, S. 2011. Mitochondria: the next (neurode)generation. *Neuron,* 70**,** 1033-53.

SCIARRETTA, C. & MINICHIELLO, L. 2010. The preparation of primary cortical neuron cultures and a practical application using immunofluorescent cytochemistry. *Methods Mol Biol,* 633**,** 221-31.

SHUTTLEWORTH, C. W. 2010. Use of NAD(P)H and flavoprotein autofluorescence transients to probe neuron and astrocyte responses to synaptic activation. *Neurochem Int,* 56**,** 379-86.

SIPOS, I., TRETTER, L. & ADAM-VIZI, V. 2003. Quantitative relationship between inhibition of respiratory complexes and formation of reactive oxygen species in isolated nerve terminals. *J Neurochem,* 84**,** 112-8.

SPINAZZI, M., CASARIN, A., PERTEGATO, V., SALVIATI, L. & ANGELINI, C. 2012. Assessment of mitochondrial respiratory chain enzymatic activities on tissues and cultured cells. *Nat Protoc,* 7**,** 1235-46.

SULZER, D. 2007. Multiple hit hypotheses for dopamine neuron loss in Parkinson's disease. *Trends Neurosci,* 30**,** 244-50.

SURIN, A. M., KHIROUG, S., GORBACHEVA, L. R., KHODOROV, B. I., PINELIS, V. G. & KHIROUG, L. 2012. Comparative analysis of cytosolic and mitochondrial ATP synthesis in embryonic and postnatal hippocampal neuronal cultures. *Front Mol Neurosci,* 5**,** 102.

SUZUKI, J., KANEMARU, K., ISHII, K., OHKURA, M., OKUBO, Y. & IINO, M. 2014. Imaging intraorganellar Ca2+ at subcellular resolution using CEPIA. *Nat Commun,* 5**,** 4153.

SUZUKI, K., KIMURA, T., SHINODA, H., BAI, G., DANIELS, M. J., ARAI, Y., NAKANO, M. & NAGAI, T. 2016. Five colour variants of bright luminescent protein for real-time multicolour bioimaging. *Nat Commun,* 7**,** 13718.

SWERDLOW, R. H., BURNS, J. M. & KHAN, S. M. 2014. The Alzheimer's disease mitochondrial cascade hypothesis: progress and perspectives. *Biochim Biophys Acta,* 1842**,** 1219-31.

TANTAMA, M., HUNG, Y. P. & YELLEN, G. 2011. Imaging intracellular pH in live cells with a genetically encoded red fluorescent protein sensor. *Journal of the American Chemical Society,* 133**,** 10034-7.

TANTAMA, M., HUNG, Y. P. & YELLEN, G. 2012. Optogenetic reporters: Fluorescent protein-based genetically encoded indicators of signaling and metabolism in the brain. *Prog Brain Res,* 196**,** 235-63.

TANTAMA, M., MARTINEZ-FRANCOIS, J. R., MONGEON, R. & YELLEN, G. 2013. Imaging energy status in live cells with a fluorescent biosensor of the intracellular ATP-to-ADP ratio. *Nature communications,* 4**,** 2550.

TAO, R., ZHAO, Y., CHU, H., WANG, A., ZHU, J., CHEN, X., ZOU, Y., SHI, M., LIU, R., SU, N., DU, J., ZHOU, H. M., ZHU, L., QIAN, X., LIU, H., LOSCALZO, J. & YANG, Y. 2017. Genetically encoded fluorescent sensors reveal dynamic regulation of NADPH metabolism. *Nat Methods*.

TREMBLAY, R. G., SIKORSKA, M., SANDHU, J. K., LANTHIER, P., RIBECCO-LUTKIEWICZ, M. & BANI-YAGHOUB, M. 2010. Differentiation of mouse Neuro 2A cells into dopamine neurons. *J Neurosci Methods,* 186**,** 60-7.

UUSITALO, L. M. & HEMPEL, N. 2012. Recent advances in intracellular and in vivo ROS sensing: focus on nanoparticle and nanotube applications. *Int J Mol Sci,* 13**,** 10660-79.

VIJAYVERGIYA, C., DE ANGELIS, D., WALTHER, M., KUHN, H., DUVOISIN, R. M., SMITH, D. H. & WIEDMANN, M. 2004. High-level expression of rabbit 15-lipoxygenase induces collapse of the mitochondrial pH gradient in cell culture. *Biochemistry,* 43**,** 15296-302.

VINCENT, A. M., MCLEAN, L. L., BACKUS, C. & FELDMAN, E. L. 2005. Short-term hyperglycemia produces oxidative damage and apoptosis in neurons. *FASEB J,* 19**,** 638-40.

WAGENER, K. C., KOLBRINK, B., DIETRICH, K., KIZINA, K. M., TERWITTE, L. S., KEMPKES, B., BAO, G. & MULLER, M. 2016. Redox Indicator Mice Stably Expressing Genetically Encoded Neuronal roGFP: Versatile Tools to Decipher Subcellular Redox Dynamics in Neuropathophysiology. *Antioxid Redox Signal,* 25**,** 41-58.

WARD, M. W., HUBER, H. J., WEISOVA, P., DUSSMANN, H., NICHOLLS, D. G. & PREHN, J. H. 2007. Mitochondrial and plasma membrane potential of cultured cerebellar neurons during glutamate-induced necrosis, apoptosis, and tolerance. *J Neurosci,* 27**,** 8238-49.

WARD, M. W., REGO, A. C., FRENGUELLI, B. G. & NICHOLLS, D. G. 2000. Mitochondrial membrane potential and glutamate excitotoxicity in cultured cerebellar granule cells. *J Neurosci,* 20**,** 7208-19.

WILL, Y., HYNES, J., OGURTSOV, V. I. & PAPKOVSKY, D. B. 2006. Analysis of mitochondrial function using phosphorescent oxygen-sensitive probes. *Nat Protoc,* 1**,** 2563-72.

WOOLLEY, J. F., STANICKA, J. & COTTER, T. G. 2013. Recent advances in reactive oxygen species measurement in biological systems. *Trends Biochem Sci,* 38**,** 556-65.

WU, J., PROLE, D. L., SHEN, Y., LIN, Z., GNANASEKARAN, A., LIU, Y., CHEN, L., ZHOU, H., CHEN, S. R., USACHEV, Y. M., TAYLOR, C. W. & CAMPBELL, R. E. 2014. Red fluorescent genetically encoded Ca2+ indicators for use in mitochondria and endoplasmic reticulum. *Biochem J,* 464**,** 13-22.

YAGINUMA, H., KAWAI, S., TABATA, K. V., TOMIYAMA, K., KAKIZUKA, A., KOMATSUZAKI, T., NOJI, H. & IMAMURA, H. 2014. Diversity in ATP concentrations in a single bacterial cell population revealed by quantitative single-cell imaging. *Sci Rep,* 4**,** 6522.

YIN, F., BOVERIS, A. & CADENAS, E. 2014. Mitochondrial energy metabolism and redox signaling in brain aging and neurodegeneration. *Antioxid Redox Signal,* 20**,** 353-71.

YOSHIDA, T., KAKIZUKA, A. & IMAMURA, H. 2016. BTeam, a Novel BRET-based Biosensor for the Accurate Quantification of ATP Concentration within Living Cells. *Sci Rep,* 6**,** 39618.

ZADRAN, S., SANCHEZ, D., ZADRAN, H., AMIGHI, A., OTINIANO, E. & WONG, K. 2013. Enhanced-acceptor fluorescence-based single cell ATP biosensor monitors ATP in heterogeneous cancer populations in real time. *Biotechnol Lett,* 35**,** 175-80.

ZHANG, L. & TRUSHINA, E. 2017. Respirometry in neurons. *Techniques to investigate mitochondrial funciton in neurons.* Springer.

ZHAO, Y., ARAKI, S., WU, J., TERAMOTO, T., CHANG, Y. F., NAKANO, M., ABDELFATTAH, A. S., FUJIWARA, M., ISHIHARA, T., NAGAI, T. & CAMPBELL, R. E. 2011a. An expanded palette of genetically encoded Ca(2)(+) indicators. *Science,* 333**,** 1888-91.

ZHAO, Y., HU, Q., CHENG, F., SU, N., WANG, A., ZOU, Y., HU, H., CHEN, X., ZHOU, H. M., HUANG, X., YANG, K., ZHU, Q., WANG, X., YI, J., ZHU, L., QIAN, X., CHEN, L., TANG, Y., LOSCALZO, J. & YANG, Y. 2015. SoNar, a Highly Responsive NAD+/NADH

Sensor, Allows High-Throughput Metabolic Screening of Anti-tumor Agents. *Cell Metab,* 21**,** 777-89.

ZHAO, Y., JIN, J., HU, Q., ZHOU, H. M., YI, J., YU, Z., XU, L., WANG, X., YANG, Y. & LOSCALZO, J. 2011b. Genetically encoded fluorescent sensors for intracellular NADH detection. *Cell Metab,* 14**,** 555-66.

ZHU, J., AJA, S., KIM, E. K., PARK, M. J., RAMAMURTHY, S., JIA, J., HU, X., GENG, P. & RONNETT, G. V. 2012. Physiological oxygen level is critical for modeling neuronal metabolism in vitro. *J Neurosci Res,* 90**,** 422-34.

ZHU, X., LEE, H. G., PERRY, G. & SMITH, M. A. 2007. Alzheimer disease, the two-hit hypothesis: an update. *Biochim Biophys Acta,* 1772**,** 494-502.

ZIELONKA, J. & KALYANARAMAN, B. 2010. Hydroethidine- and MitoSOX-derived red fluorescence is not a reliable indicator of intracellular superoxide formation: another inconvenient truth. *Free Radic Biol Med,* 48**,** 983-1001.

12. Figure Legends